

# The Palmitoylation Machinery Is a Spatially Organizing System for Peripheral Membrane Proteins

Oliver Rocks,<sup>1,2,6,7</sup> Marc Gerauer,<sup>3,5,6</sup> Nachiket Vartak,<sup>2</sup> Sebastian Koch,<sup>3,5</sup> Zhi-Ping Huang,<sup>3</sup> Markos Pechlivanis,<sup>4</sup> Jürgen Kuhlmann,<sup>4</sup> Lucas Brunsved,<sup>3,5</sup> Anchal Chandra,<sup>2</sup> Bernhard Ellinger,<sup>3</sup> Herbert Waldmann,<sup>3,5,\*</sup> and Philippe I.H. Bastiaens<sup>1,2,5,\*</sup>

<sup>1</sup>European Molecular Biology Laboratory, Meyerhofstrasse 1, 69118 Heidelberg, Germany

<sup>2</sup>Department of Systemic Cell Biology

<sup>3</sup>Department of Chemical Biology

<sup>4</sup>Department of Structural Biology

Max Planck Institute for Molecular Physiology, Otto-Hahn-Strasse 11, 44227 Dortmund, Germany

<sup>5</sup>TU Dortmund, Fachbereich Chemie, 44227 Dortmund, Germany

<sup>6</sup>These authors contributed equally to this work

<sup>7</sup>Present address: Samuel Lunenfeld Research Institute, Mount Sinai Hospital, 600 University Avenue, Toronto, Ontario M5G 1X5, Canada

\*Correspondence: [herbert.waldmann@mpi-dortmund.mpg.de](mailto:herbert.waldmann@mpi-dortmund.mpg.de) (H.W.), [philippe.bastiaens@mpi-dortmund.mpg.de](mailto:philippe.bastiaens@mpi-dortmund.mpg.de) (P.I.H.B.)

DOI 10.1016/j.cell.2010.04.007

## SUMMARY

Reversible S-palmitoylation of cysteine residues critically controls transient membrane tethering of peripheral membrane proteins. Little is known about how the palmitoylation machinery governs their defined localization and function. We monitored the spatially resolved reaction dynamics and substrate specificity of the core mammalian palmitoylation machinery using semisynthetic substrates. Palmitoylation is detectable only on the Golgi, whereas depalmitoylation occurs everywhere in the cell. The reactions are not stereoselective and lack any primary consensus sequence, demonstrating that substrate specificity is not essential for de-/repalmitoylation. Both palmitate attachment and removal require seconds to accomplish. This reaction topography and rapid kinetics allows the continuous redirection of mislocalized proteins via the post-Golgi sorting apparatus. Unidirectional secretion ensures the maintenance of a proper steady-state protein distribution between the Golgi and the plasma membrane, which are continuous with endosomes. This generic spatially organizing system differs from conventional receptor-mediated targeting mechanisms and efficiently counteracts entropy-driven redistribution of palmitoylated peripheral membrane proteins over all membranes.

## INTRODUCTION

S-palmitoylation of cysteine residues is a common posttranslational modification found on integral and peripheral membrane

proteins, many of which are central elements in signal transduction, synaptic function, or membrane trafficking and fusion (Bijlmakers and Marsh, 2003; Smotrys and Linder, 2004). Palmitoylation can promote stable tethering of otherwise cytosolic proteins to intracellular membranes, can contribute to altered anterograde and endocytic trafficking of integral membrane proteins (Charollais and Van Der Goot, 2009), and, for both, can account for their lateral segregation into lipid microdomains (Melkonian et al., 1999). Palmitoylation is the only reversible lipid modification (Magee et al., 1987). Cycles of de- and reacylation govern the transient membrane association of peripheral membrane proteins and thereby regulate their steady-state localization, sorting, and function (Greaves and Chamberlain, 2007; Huang and El-Husseini, 2005; Rocks et al., 2006). However, the parameters and rules that determine the localization of peripheral membrane proteins via palmitoylation and depalmitoylation in cells are unclear. Palmitoylation activity was assigned to several membrane compartments (El-Husseini et al., 2002; Fishburn et al., 1999; Rocks et al., 2005; Swarthout et al., 2005; van't Hof and Resh, 1997), and depalmitoylation was shown to occur at least at the plasma membrane (PM) (El-Husseini et al., 2002; Rocks et al., 2005) and estimated palmitate turnover kinetics range from 1 hr (Baker et al., 2003; Lu and Hofmann, 1995) to a few minutes (Rocks et al., 2005). Both enzymatic and nonenzymatic mechanisms of palmitoylation were proposed. It occurs spontaneously *in vitro* (Baño et al., 1998; Quesnel and Silvius, 1994) and targets the same cysteines that are palmitoylated in cells. Structural integrity of the substrate is not required since palmitate is also transferred to corresponding short peptides (Baño et al., 1998; Bizzozero et al., 2001; Quesnel and Silvius, 1994). Recently, protein acyltransferases (PATs) were identified in yeast and subsequently in the human genome, most notably the 25 members of the mammalian DHHC protein family (Mitchell et al., 2006). For individual candidate PATs apparent substrate selectivity was reported (Linder and Deschenes, 2007; Tsutsumi et al., 2008), but a consensus

sequence for S-palmitoylation has not yet been identified (Bijlmakers and Marsh, 2003; Smotrys and Linder, 2004). In a proteomic screen in yeast (Roth et al., 2006), both discrete and overlapping functionalities among the candidate PATs were shown. Acyl protein thioesterase 1 (APT-1) currently is the only thioesterase activity (TE) known to depalmitoylate in vivo (Zeidman et al., 2009) (P.I.H.B. and H.W., unpublished data).

Here, we delineate the critical parameters that govern the spatial organization of palmitoylated peripheral membrane proteins. By monitoring the turnover kinetics of semi-synthetic PAT/TE substrate proteins that we introduce into cells, we determine the localization, efficiency, and specificity of the core mammalian palmitoylation machinery.

## RESULTS

### Monolipidated Substrates for S-Palmitoylation Rapidly and Randomly Partition over All Membranes

Palmitoylated peripheral membrane proteins typically contain an irreversibly attached prenyl or myristoyl moiety in proximity to the palmitoylation site. We first questioned whether singly lipidated proteins exhibit a specific membrane distribution to facilitate their subsequent S-palmitoylation. Mutant solely farnesylated HRasC181,C184S and solely myristoylated MyrSer (32 aa peptide [Navarro-Lérida et al., 2002]) that cannot get palmitoylated were equipped with mCherry and mCitrine, respectively, to observe their steady-state localization. In both cases, the fluorescence distribution did not show a preference for any membrane compartment, but merely reflected membrane densities (Figure 1A). Photoactivatable GFP-fused versions of both proteins rapidly redistributed over all membranes, reaching steady-state within the first seconds after photoactivation (Figures 1B and 1C). In order to confirm that the monolipidated proteins also had access to the PM, TIRF microscopy was performed on the wild-type and monolipidated mutant proteins. As expected, the fully lipidated wild-type proteins clearly showed an enrichment at the PM (Figure 1D). However, both monolipidated mutants also exhibited clear PM localization, establishing that they have access to this membrane. These experiments are inconsistent with the presence of receptors for monolipidated proteins on specific membrane compartments (Choy et al., 1999). Instead, proteins with only one attached lipid rapidly and randomly sample all membranes until they are trapped because of an increase in their affinity for membranes by the acquisition of additional lipid anchors at the site of palmitoylation. This kinetic trapping (Shahinian and Silvius, 1995) is an essential aspect of the spatial organization of palmitoylated peripheral membrane proteins that can be exploited to detect the subcellular site of palmitoylation.

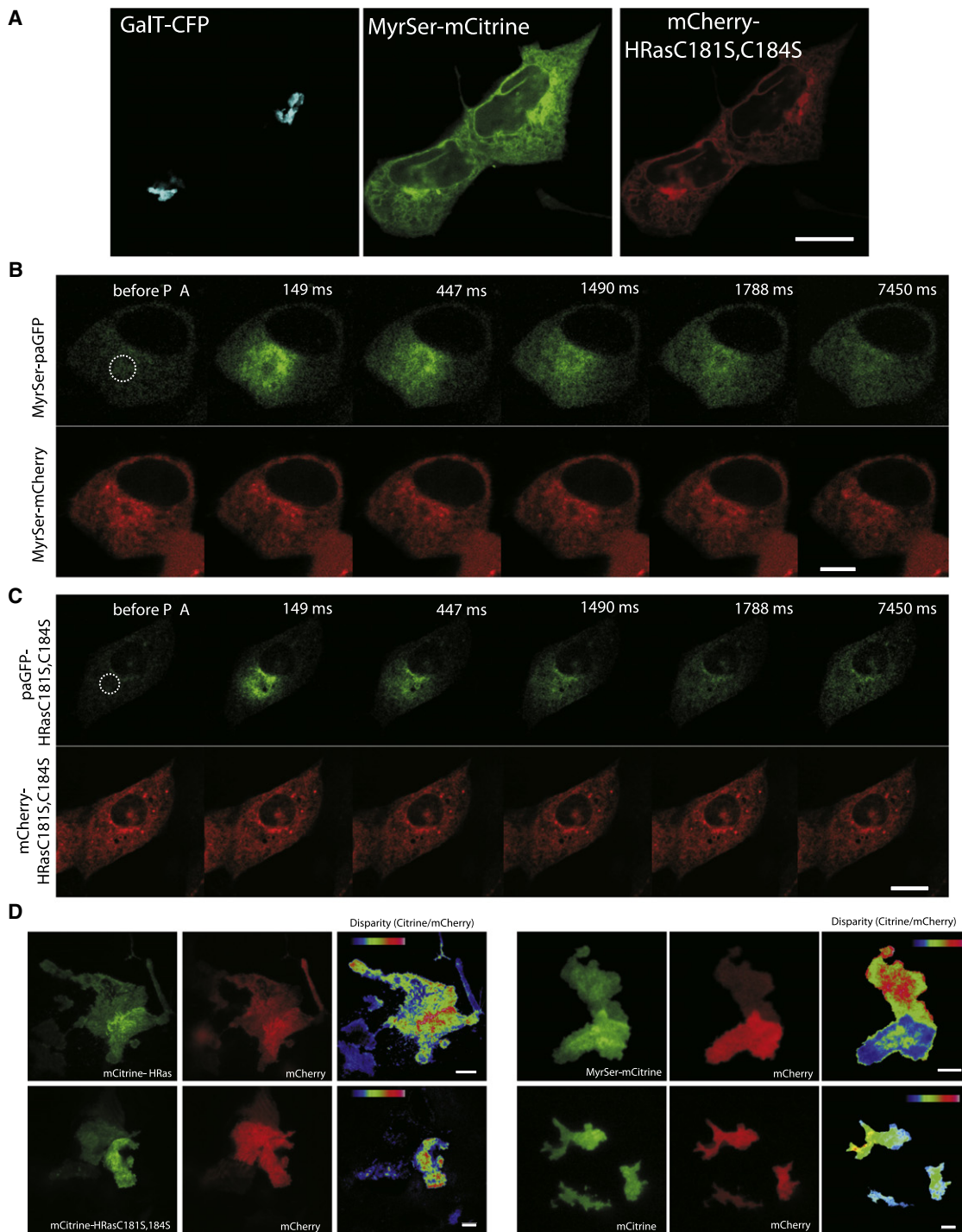
### Subcellular Localization and Kinetics of Ras Palmitoylation

We prepared a set of semisynthetic NRas proteins that feature differentially lipid-modified heptapeptides ligated to fluorescently labeled recombinant NRas(1–181). This was achieved by employing a combination of solid phase lipopeptide synthesis and peptide-protein ligation (Figure 2A, Figure S1 available online) (Kuhn et al., 2001). After introduction of these probes

into living cells, we directly monitored their spatially resolved palmitate turnover kinetics by making use of the phenomenon of kinetic trapping (Shahinian and Silvius, 1995) that is apparent from a local probe accumulation caused by a decrease in effective diffusion. We investigated the subcellular site and the kinetics of Ras palmitoylation using CysFar, a substrate for acylation resembling depalmitoylated NRas (Figure 2A). This solely farnesylated protein rapidly distributed over all membranes directly after injection (Figure 2B), similar to palmitoylation-deficient but farnesylated HRasC181,C184S (Figures 1A and 1C). At the same time, stable membrane anchoring of the probe at the site of palmitoylation was apparent as rapid accumulation of CysFar specifically at the Golgi with a  $t/2$  of  $14 \pm 8.4$  s ( $n = 9$ , Figures 2B and 2C). Only at later time points a fluorescence increase at the PM could be observed showing that Golgi exit of the palmitoylated probe via the secretory pathway (Figure S2A) accounts for enrichment of palmitoylated Ras at the PM (Choy et al., 1999). In contrast, SerFar, a probe that cannot undergo palmitoylation, nonspecifically distributed over endomembranes (Figures 2A, 2D, and 2E upper panel). This was also observed for CysFar after blocking the cysteine with N-ethylmaleimide (Figure S2B). Photobleaching of SerFar at the Golgi resulted in rapid fluorescence recovery within seconds, comparable to the redistribution of palmitoylation-deficient HRasC181S,C184S (Figure 2E, lower panel). In contrast, CysFar fluorescence recovery at the Golgi was 13-fold slower ( $t/2 = 29 \pm 6.8$  s,  $n = 7$ ), showing that its Golgi pool is more stably membrane anchored as a result of palmitoylation. In cells pretreated with 2-bromopalmitate, which inhibits palmitic acid biosynthesis and thereby indirectly protein palmitoylation (Webb et al., 2000), specific Golgi enrichment of CysFar was blocked (Figure 2F). Similar rapid and specific accumulation of CysFar on the Golgi was observed in COS7 and MCF7 cells (data not shown). We conclude that palmitoylation of the carboxy-terminal prenylated substrate protein Ras occurs on the time scale of seconds and is confined to the surface of the Golgi apparatus.

### Palmitoylation of Peripheral Membrane Proteins at the Golgi

In order to investigate the generality of the Golgi as palmitoylation site, we asked whether the two other classes of cytosolic palmitoylatable substrates in mammals, i.e., proteins that are N-myristoylated and S-palmitoylated at the N terminus and proteins that are only S-palmitoylated (Bijlmakers and Marsh, 2003), undergo similar rapid palmitoylation at the Golgi. We tested semisynthetic Gαi1Cys, an amino-terminal palmitoylatable substrate embodying a N-myristoylated heptapeptide derived from the heterotrimeric G protein alpha i1 subunit, and semisynthetic GAP43Cys, comprising the first 20 amino acids of GAP43 including its two palmitoylatable cysteines (Figure 3A). Gαi1Cys exhibited Golgi accumulation characteristics ( $t/2 = 21 \pm 11$  s,  $n = 6$ ) comparable to CysFar and became enriched at the PM also only later after injection. Local membrane trapping was blocked by replacement of the target cysteine with serine or by the presence of 2-bromopalmitate (Figures 3B and 3C, Figure S3). GAP43 lacks additional lipid anchors and might gain access to the palmitoylation machinery by a weak intrinsic

**Figure 1. Rapid and Random Partitioning of Monolipidated Proteins**

(A) Steady-state localization of MyrSer is similar to that of HRasC181S,C184S.

(B and C) Fluorescence loss of photoactivated MyrSer-paGFP (B) and paGFP-HRasC181S,C184S (C) at the perinuclear region in MDCK cells, showing that both single lipidated proteins rapidly and indiscriminately sample different cellular membrane systems with comparable membrane residence times. PA, photoactivation.

(D) Total internal reflection fluorescence (TIRF) images of MDCK cells expressing Citrine-HRas or Citrine-HRasC181S,C184S and MyrSer-Citrine. The fluorescence signals from the lipidated proteins were normalized to soluble mCherry to show the disparity in contrast reflecting their PM localization. Free mCitrine/mCherry images are shown as controls, showing disparity arising due to differences in optical parameters of the TIRF field.

Scale bars represent 10  $\mu$ M. Color bar indicates normalized range of pixel ratios from minimum (blue) to maximum (red).

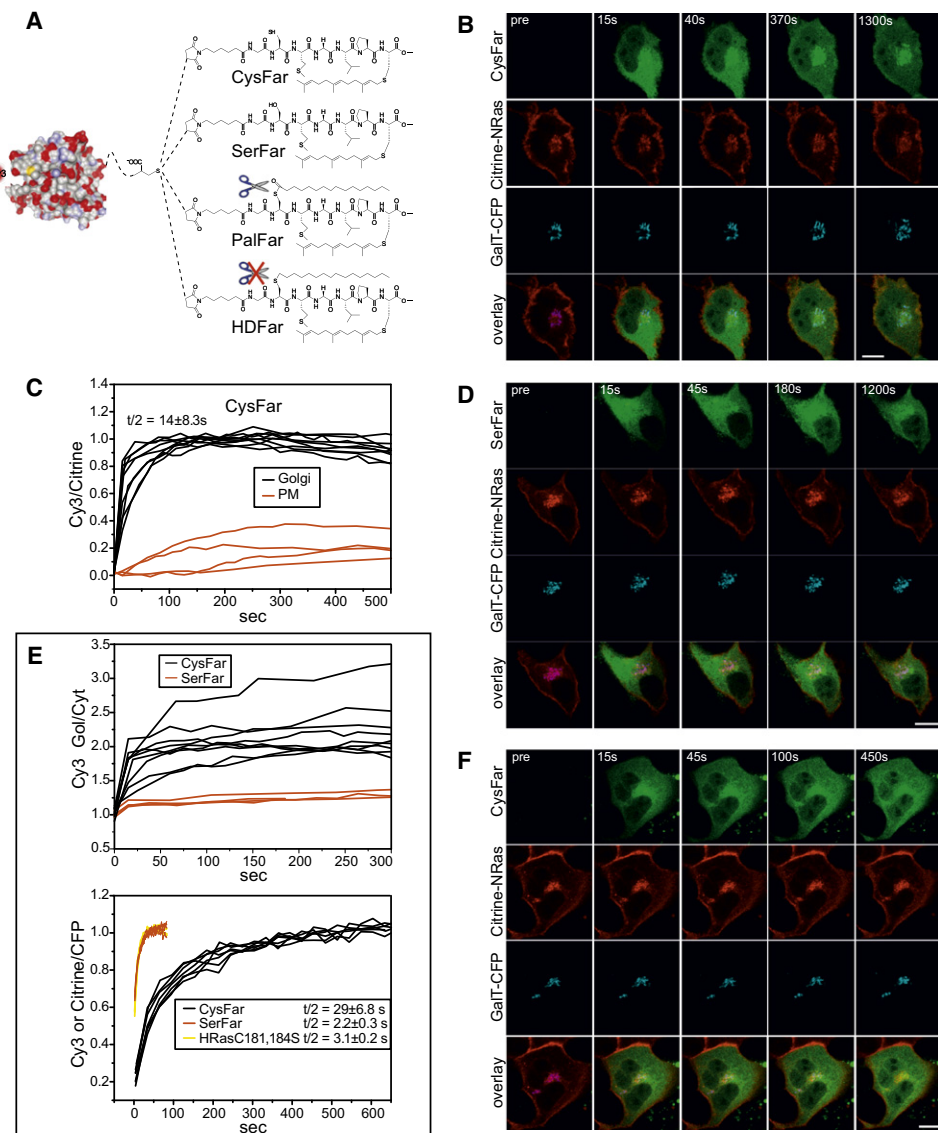


**Figure 2. Ras Palmitoylation Is Fast and Restricted to the Golgi**

- (A) Schematic illustration of the Cy3-labeled semisynthetic lipoproteins. Different lipopeptide-heptamers were coupled via a maleimidocaproyl linker to recombinant NRas (1–181).
- (B) Confocal time-lapse images of MDCK cells transiently expressing the Golgi marker GaIT-CFP and Citrine-NRas prior and after microinjection of CysFar.
- (C) Quantitative ratiometric analysis of CysFar accumulation at the Golgi (black, n = 9) and the PM (red, n = 4) with local Citrine-NRas intensity used as reference. Plateau fluorescence ratios at the Golgi were normalized to one.
- (D) Time-lapse images of MDCK cells microinjected with nonpalmitoylatable SerFar.
- (E) Top: contrast of SerFar fluorescence at the Golgi over adjacent membranes and cytosol (red, n = 4) compared to CysFar (black, n = 9). Bottom: fluorescence recovery after selective photobleaching of SerFar (red, n = 5) or CysFar (black, n = 7) at the Golgi 5 min after microinjection. The recovery of local fluorescence was ratiometrically quantified with Citrine-NRas used as a Golgi reference. Results were compared to Golgi photobleaching data of Citrine-HRasC181,184S (yellow, n = 3) in cells coexpressing CFP-NRas as a Golgi reference. Plateau values were normalized to one.
- (F) Microinjection of CysFar in MDCK cells preincubated with 50 μM 2-bromopalmitate for 45 min.

All scale bars represent 10 μm. See also Figures S1 and S2.

membrane affinity (El-Husseini et al., 2000; Greaves et al., 2009). GAP43Cys, but not a serine double mutant, accumulated specifically on the Golgi but not on any other cellular membrane ( $t_{1/2} = 29 \pm 15$  s, n = 7, Figures 3C and 3D, Figure S4A), similar to CysFar.

We also studied a probe comprising the amino-terminal N-myristoylated heptapeptide of the Fyn kinase that was previously shown to be palmitoylated at the PM (van't Hof and Resh, 1997). FynCys, but not a serine double mutant, accumulated initially only at the Golgi ( $t_{1/2} = 16 \pm 4.2$  s, n = 5,

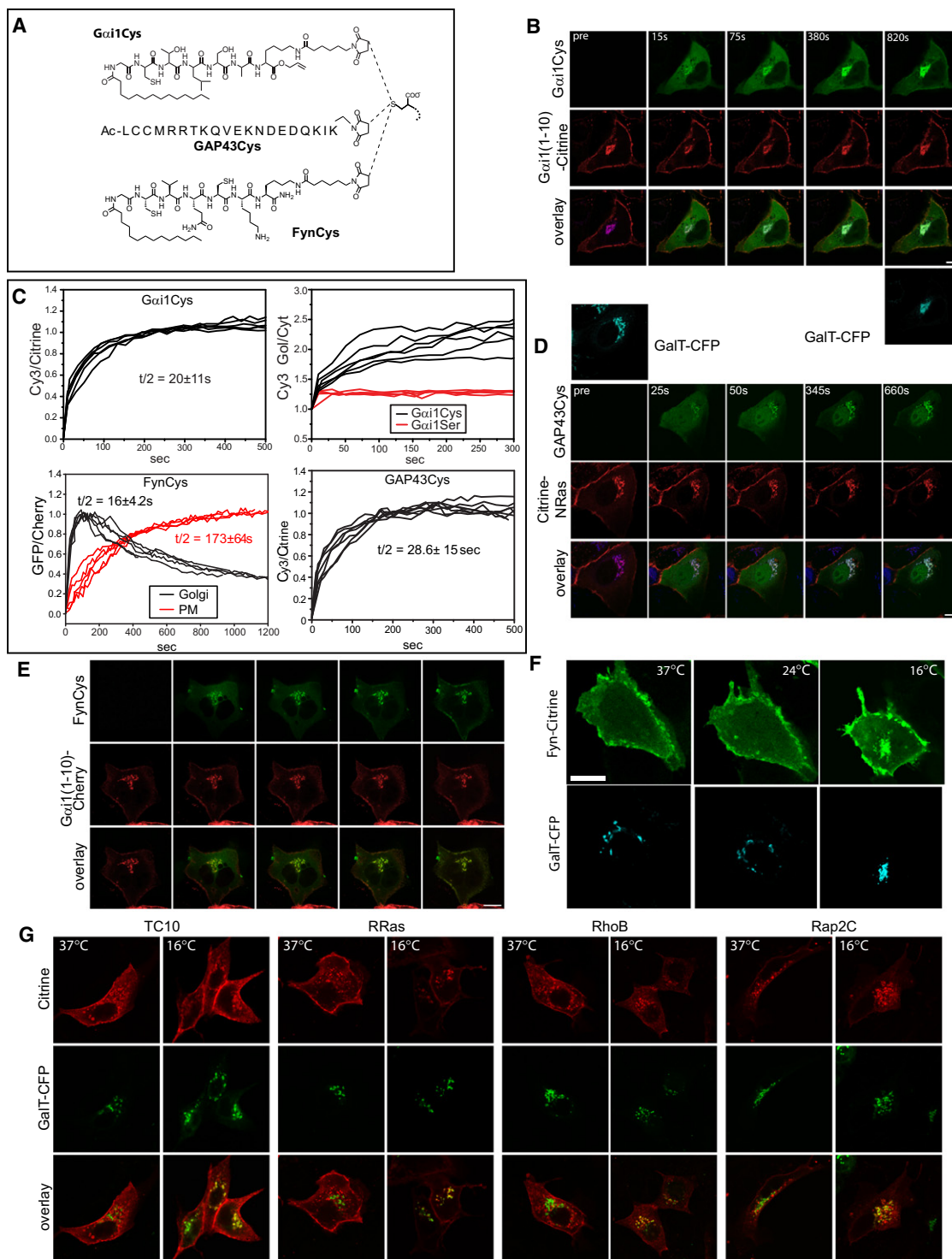


**Figure 3. Rapid palmitoylation of different classes of substrates on the Golgi**

(A) Schematic illustration of the peptide portions of Gαi1Cys (featuring a palmitoylatable N-myristoylated heptapeptide derived from the amino-terminus of Gαi1) and of GAP43Cys (featuring the first 20 amino acids of GAP43, including two palmitoylatable cysteines) mounted to Cy3-labeled recombinant NRas (1–181) and of FynCys (featuring a doubly palmitoylatable N-myristoylated heptapeptide derived from the amino-terminus of Fyn kinase) mounted to recombinant GFP.

(B) Confocal time-lapse images of MDCK cells microinjected with Gαi1Cys transiently expressing both the Golgi marker GalT-CFP and Citrine fused to the first ten amino acids of Gαi1.

(C) Top: quantitative ratiometric analysis of Gαi1Cys accumulation at the Golgi ( $n = 6$ ) and contrast of Gαi1Ser fluorescence at the Golgi over adjacent membranes and cytosol (red,  $n = 4$ ) compared to Gαi1Cys (black,  $n = 6$ ). Bottom: quantitative ratiometric analysis of FynCysGFP accumulation at the Golgi (black  $n = 5$ ) and at

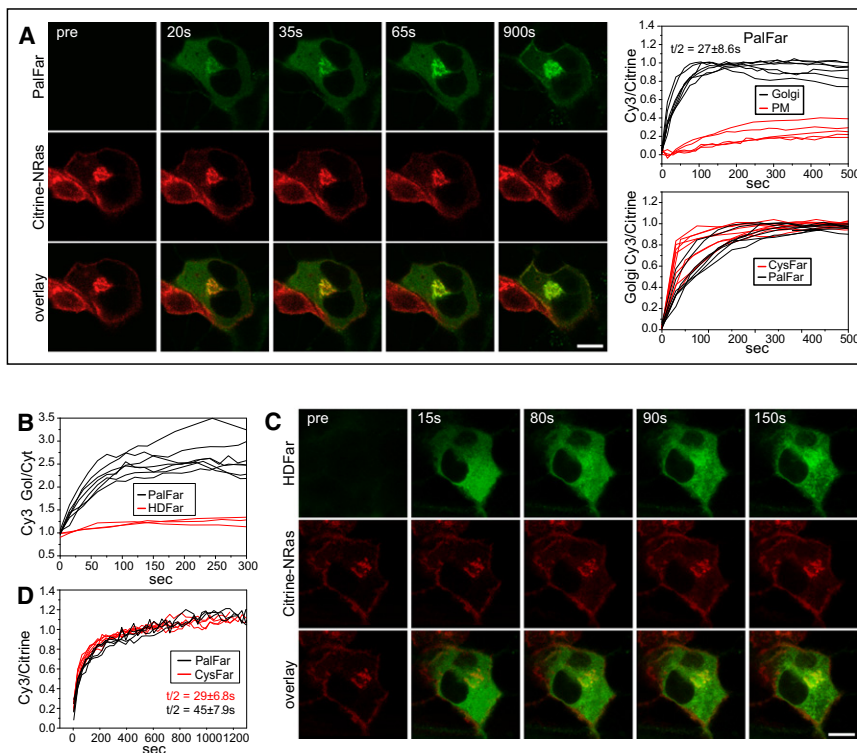


**Figure 4. Rapid Depalmitoylation on All Membranes**

(A) Left: confocal time-lapse images of MDCK cells expressing Citrine-NRas microinjected with PalFar. Top right: quantitative analysis of PalFar accumulation at the Golgi (black,  $n = 7$ ) and the PM (red,  $n = 5$ ) with local Citrine-NRas intensity used as reference. Bottom right: comparison of Golgi accumulation kinetics of microinjected PalFar (black,  $n = 7$ ) and CysFar (red,  $n = 9$ ).

(B) Contrast of PalFar fluorescence at the Golgi over adjacent membranes and cytosol (black,  $n = 7$ ) compared to HDFar (red,  $n = 3$ ).

(C) Confocal time-lapse images of MDCK cells expressing Citrine-NRas microinjected with non-depalmitoylatable HDFar.

(D) Fluorescence recovery after selective photo-bleaching of PalFar at the Golgi (black,  $n = 5$ ) compared to CysFar (red,  $n = 7$ ) shortly after microinjection. Recovery was ratiometrically quantified with local Citrine-NRas fluorescence intensity used as reference.

All scale bars represent 10  $\mu$ m. See also Figure S5.

Figures 3A, 3C, and 3E, Figure S4B) but not at the PM. Only at later time points enrichment of the probe at the PM occurred due to anterograde transport of palmitoylated probe via the secretory pathway ( $t/2 = 173 \pm 64$  s,  $n = 5$ ). Interestingly, the PM localization of FynCys at steady state was more pronounced than that for the other probes. The longer membrane residence time of this probe indicates lower palmitate turnover kinetics, similar to those that can be imposed on HRas by increasing the number of palmitoylated cysteine residues through mutagenesis (Figure 3C; see below). This explains why genetically expressed full-length Fyn or Fyn(1–11) mostly localize at the PM. As expected, but contrary to a recent study (Sato et al., 2009), temperature block of anterograde vesicular transport shifts the steady-state distribution of Fyn back toward the Golgi (Figure 3F). Various other palmitoylated peripheral membrane proteins do not exhibit clear Golgi localization, implying that they are palmitoylated on other membrane systems. Prenylated and palmitoylated RhoB, TC10, RRas, and Rap2C typically decorate the endocytic and/or lysosomal compartment along with the PM (Kawase et al., 2006; Paganini et al., 2006; Pérez-Sala et al.,

2009; Takaya et al., 2007). We tested whether palmitoylation of these proteins nevertheless occurs on the Golgi. Indeed, a temperature block of vesicular transport resulted in a robust shift of their steady-state localization to the Golgi (Figure 3G). This also shows that these proteins exhibit a slower palmitate turnover, which allows them to reach the endocytic compartment via the PM. The above experiments with representative substrates of all three classes of peripheral membrane proteins, together with the data shown in Figure 2, demonstrate that the surface of the Golgi is the predominant subcellular site of peripheral membrane protein palmitoylation in mammalian cells. It provides directionality to the acylation cycle by making use of the secretory functionality of the Golgi that targets the PM.

#### Homogeneous Protein Depalmitoylation

We then studied palmitate removal in cells in order to understand how the overall palmitoylation machinery controls protein localization. First, we analyzed the depalmitoylation kinetics of PalFar, a substrate for palmitate removal resembling fully lipid modified NRas (Figure 2A). PalFar rapidly accumulated on the Golgi shortly after microinjection (Figures 4A and 4B, Figure S5A) with a  $t/2$  of  $27 \pm 8.6$  s ( $n = 7$ ), which is only marginally slower than CysFar. This probe is expected to insert into all

the PM ( $n = 5$ , red), using local Gαi1(1–10)-Cherry intensity as reference. Plateau values were normalized to one. Quantitative ratiometric analysis of GAP43Cys accumulation at the Golgi ( $n = 7$ ).

(D) Confocal time-lapse images of MDCK cells microinjected with GAP43Cys expressing both the Golgi marker GaT-CFP and Citrine-NRas. Note that the lack of additional lipid anchors allows for nuclear diffusion of unprocessed probe.

(E) Time-lapse images of MDCK cells microinjected with FynCys-GFP expressing Gαi1-Cherry.

(F) Vesicular transport block at 16°C (1 hr incubation) shifts the steady state distribution of WT Fyn to the Golgi apparatus in MDCK cells.

(G) Confocal images of the steady-state localization of various prenylated and palmitoylated proteins in fixed MDCK cells at 37°C or after temperature block at 16°C for 10 hr.

All scale bars represent 10  $\mu$ m. See also Figures S3, S4, and S6.

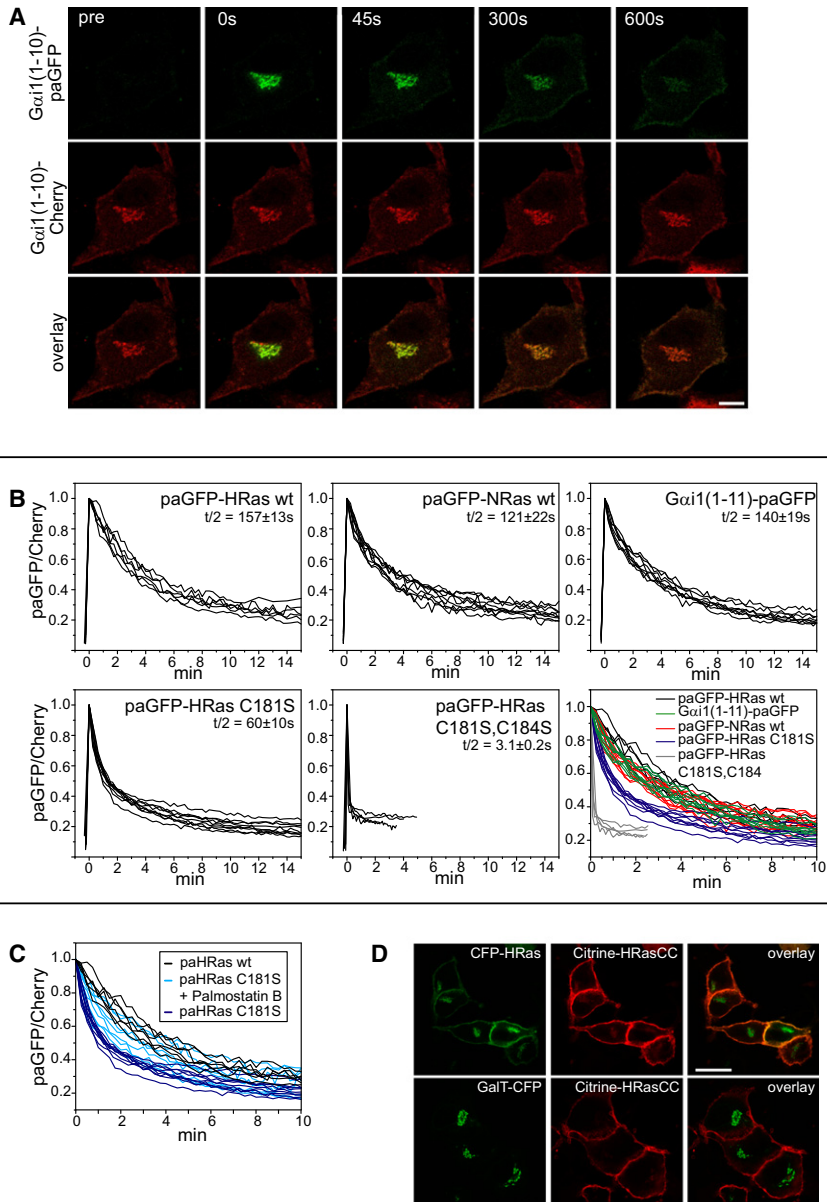


**Figure 5. Depalmitoylation Is a Fully Distributed Process**

(A) Time-lapse images of MDCK cells expressing Gαi1(1-10) fused to paGFP and Gαi1(1-10) fused to mCherry. paGFP was selectively photoactivated at the Golgi by short illumination with 405 nm laser light. Images were taken before and after photoconversion at the indicated time points. The scale bar represents 10 μm. For information on palmitoylation kinetics of an injected Gαi-heptapeptide GFP fusion probe, see Figure S6.

(B) Ratiometrically determined decrease of paGFP fluorescence at the Golgi after photoconversion of the palmitoylated fusion proteins HRas ( $n = 6$ ), NRas ( $n = 9$ ), Gαi1(1-10) ( $n = 8$ ) and HRasC181S ( $n = 9$ ), or of solely farnesylated HRasC181,184S ( $n = 5$ ). Peak values were normalized to one. An overlay of all curves is displayed in the lower-right graph.

(C) Ratiometrically determined decrease of paGFP-HRasC181S fluorescence at the Golgi after photoconversion in presence or absence of 1 μM palmostatin B for 45 min, compared to paGFP-HRas in untreated cells.

(D) Confocal images of MDCK cells expressing Citrine-HRas179C183C containing four potential palmitoylation sites together with wild-type CFP-HRas (upper panel) or GaIT-CFP (lower panel). Scale bars represent 25 μm.

inhibited specific Golgi accumulation of PalFar (Figure S5C). These experiments demonstrate that both palmitylation and depalmitoylation in cells occur within seconds and are thus at least two orders of magnitude faster than previously concluded from pulse-chase experiments (Baker et al., 2003; Linder and Deschenes, 2007; Lu and Hofmann, 1995). In a complementary approach, we assessed whether depalmitoylation occurs as early in the acylation cycle as at the Golgi, thereby showing that it is a fully distributed process. For this, palmitoylatable constructs with different palmit-

cellular membranes after microinjection, where it remains stably tethered: a situation reflected by the nonspecific membrane localization of a PalFar analog that cannot undergo de-/repalmitoylation because of a noncleavable thioether bond (HDFar, Figures 2A, 4B, and 4C). This shows that depalmitoylation efficiently releases PalFar from all membranes before rapid diffusion and repalmitoylation results in its membrane trapping on the Golgi. PalFar also appeared at the PM a few minutes after injection as a result of anterograde transport of probe that had been repalmitoylated on the Golgi (Figure 4A, Figures S5A and S5B). Photobleaching recovery kinetics of PalFar at the Golgi were similar to CysFar (Figure 4D), confirming that PalFar was indeed depalmitoylated when reaching the Golgi, thereby showing that the injected probe is accessible for palmitate removal everywhere in the cell. 2-bromopalmitate treatment

tate turnover rates (Lu and Hofmann, 1995; Rocks et al., 2005) fused to photoactivatable GFP were expressed. The probes were selectively photoactivated on the Golgi and the decrease in local fluorescence was followed over time (Figures 5A and 5B). Because we are photoactivating material at the Golgi, the relative decrease of local fluorescence is only affected by the clearance rate constant ( $k_c$ ). The observed residence time ( $t_{1/2} = 1/k_c$ ) will be the inverse of the sum of the rate constant of clearance by the secretory pathway and the rate constant of clearance by depalmitoylation and subsequent diffusive loss. If there is no depalmitoylation at the Golgi, the observed residence time will only depend on the secretory pathway and should therefore be the same for all tested palmitoylated molecules. However, a clear correlation was found between the residence time of these proteins on the Golgi and their kinetics

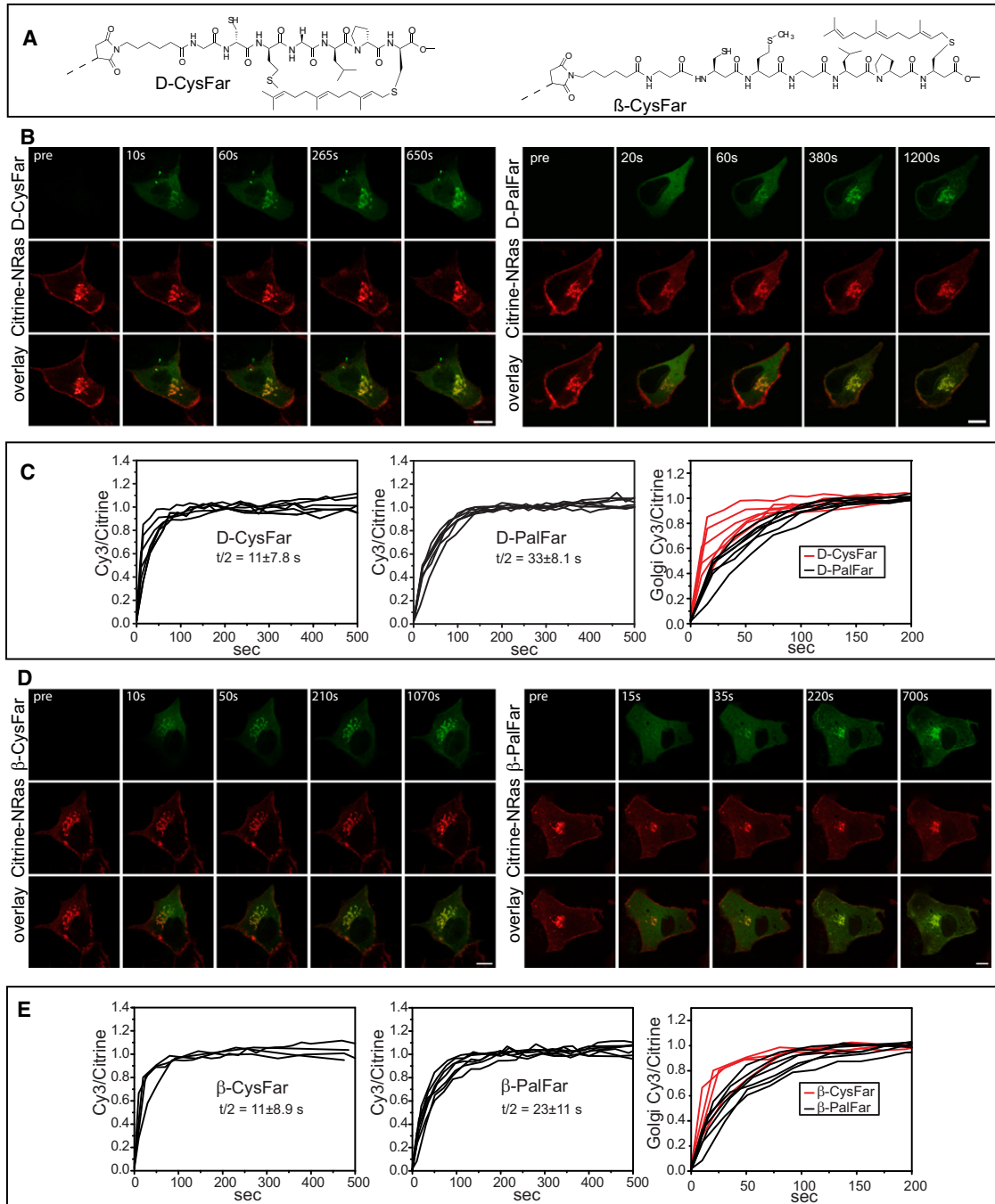
of palmitate turnover (see Figure S6): fluorescence decay of double palmitoylated and farnesylated paGFP-HRas was slowest ( $t/2: 157 \pm 13$  s,  $n = 6$ ), followed by monopalmitoylated and myristoylated paGFP-G $\alpha$ 1 (aa 1–11;  $t/2: 140 \pm 19$  s,  $n = 8$ ) and monopalmitoylated and farnesylated paGFP-NRas ( $t/2: 121 \pm 22$  s,  $n = 9$ ), while the fastest fluorescence decay was observed for monopalmitoylated and farnesylated paGFP-HRasC181S ( $t/2: 60 \pm 10$  s,  $n = 9$ ). As a control, nonpalmitoylatable paGFP-HRasC181,184S rapidly decayed within a few seconds. Importantly, the rate constants of Golgi clearance for the monopalmitoylated C181S mutant and double-palmitoylated wild-type HRas converged in presence of palmostatin B, an inhibitor of depalmitoylation (P.I.H.B. and H.W., unpublished data), demonstrating that the differently palmitoylated probes are indeed indiscriminately sorted into Golgi exit vesicles (Figure 5C). The correlation between the kinetics of palmitate removal and Golgi residence time clearly shows that palmitate removal already takes place at the Golgi. In fact, the depletion of paGFP-HRasC181S from the Golgi is more than one order of magnitude faster than the reported time scale of vesicle release into the secretory pathway (Hirschberg et al., 1998). Palmitate removal on the secretory pathway/Golgi prevents a substantial fraction of palmitoylated proteins from reaching the PM, since it redirects these proteins into the acylation cycle before they can reach the PM via the secretory pathway. This short circuit in the transport cycle affects the relative steady state PM/Golgi partitioning of a palmitoylated protein and causes a stronger uncoupling of the endomembrane protein pool from the PM compartment. Indeed, incorporation of two additional palmitoylation sites to the HRas carboxy-terminus (HRas179C,183C) results in a more pronounced steady-state PM localization (Figure 5D), as expected for a protein with slower apparent palmitate turnover kinetics.

### Substrate Specificity of the Core Palmitoylation Machinery

We have shown that the spatial organization of palmitoylated peripheral membrane proteins is controlled by the topographic organization of the de-/reacylation machinery and its high processivity. We then investigated whether the resulting specificity in localization is achieved by a generic—i.e., nonspecific—overall palmitoylation mechanism. Proteins are chiral catalysts and their selectivity to a major extent is based on recognizing the chirality of their substrates. We therefore converted CysFar and PalFar into their stereoisomeric counterparts with amino acid configuration altered in the immediate vicinity of the palmitoylation site as an utmost test of the stereotolerance of both lipidation and delipidation. *D*-CysFar and *D*-PalFar are semisynthetic proteins that resemble CysFar and PalFar in their side-chain functionality but feature the last seven carboxy-terminal amino acids in nonnatural *D*-configuration (Figure 6A). Thereby, secondary recognition sites in the palmitoylation and depalmitoylation reaction in vicinity to the target cysteine are likely to be disrupted. However, both *D*-CysFar and *D*-PalFar rapidly accumulated on the Golgi, with kinetics indistinguishable from their *L*-configured counterparts (Figures 6B and 6C). This demonstrates that the core cellular palmitoylation and depalmitoylation machinery is not stereoselective. We asked whether palmitate transfer or removal

requires any form of molecular recognition at all of structural patterns in vicinity to the target cysteine. Semisynthetic  $\beta$ -CysFar and  $\beta$ -PalFar feature heptapeptides made of  $\beta$  amino acids that contain an additional carbon atom between the amino and carboxy groups (Figure 6A) (Seebach et al., 2004). These modifications do not affect the integrity of the side chains but at most alter the secondary structure of the carboxy-terminus of the probe, including the target cysteine itself. Moreover, the  $\beta$  peptide backbone is one-third longer than the natural counterpart heptapeptide. Both microinjected  $\beta$ -CysFar and  $\beta$ -PalFar were rapidly trapped on the Golgi by palmitoylation with kinetics similar to CysFar or PalFar, respectively (Figures 6D and 6E). We therefore conclude that no consensus sequence is involved in cellular palmitoylation and that there is no essential requirement for the de-/repalmitoylation machinery to recognize any structure on the substrate other than the target cysteine side chain. The above experiments also confirm the central role of the Golgi in cellular palmitoylation and thereby reveal the generic nature of the spatially organizing system that is constituted by the two lipid modifying activities. The specific Golgi accumulation of all probes was blocked in the presence of 2-bromopalmitate (data not shown).

We investigated the involvement of offsite recognition in palmitoyl turnover of our probes via putative motifs on the Ras-G-domain distal to the target cysteine. First, YFP-tH, a YFP fusion of the minimal C-terminal membrane targeting sequence of HRas (aa 175–190) and full-length mCherry-HRas exhibited an identical steady-state partitioning over the PM and the Golgi (Figure 7A). They therefore must have identical palmitoyl turnover kinetics arguing against recognition of the Ras G-domain by the palmitoylation machinery. Second, G $\alpha$ i1Cys-GFP, a probe where the amino-terminal G $\alpha$ i1 heptapeptide is coupled to GFP instead of truncated NRas, displayed kinetics of Golgi accumulation similar to G $\alpha$ i1Cys ( $t/2 = 18 \pm 5$  s,  $n = 5$ ), showing that the NRas protein core is dispensable for the recognition of the heptapeptide substrate by the palmitoylation machinery (Figure S6; see also Figures 3C and 3E). Finally, we investigated whether any specificity for the palmitoylation reaction resided in the DHHC domain-containing proteins. Previous studies have suggested that the DHHC PATs have distinct, albeit overlapping, specificities (Linder and Deschenes, 2007; Roth et al., 2006; Tsutsumi et al., 2008). Human DHHC9 and Yeast Erf2 have so far been identified as RasPATs on the basis of biochemical assays (Lobo et al., 2002; Swarthout et al., 2005), and evidence also exists for DHHC17 and 18 (Fukata et al., 2004; Huang et al., 2004). However, short hairpin RNA (shRNA)-mediated knockdown of DHHC9 showed no detectable effect on Ras palmitoylation, as evident from a steady steady-state localization and recovery kinetics of HRas photobleached at the Golgi that are similar to control cells (Figures 7B–7D). We therefore used a Hidden Markov Model (HMM)-based bioinformatics approach (Smyth, 1997) to classify the 25 human DHHC proteins into different classes on the basis of biochemical data indicating their preferred protein substrates (Extended Experimental Procedures). Indeed, the HMM indicated closer relationships (Figure S7A) between these particular DHHC proteins with the consensus sequence “W-X(4)-L-X(12)-TTNE” in mammalian and yeast proteins (Figure S7B) that was correlated with RasPAT

**Figure 6. Substrate Tolerance of the Palmitoylation Machinery**(A) Schematic illustration of the heptapeptide portions of semisynthetic D-CysFar and  $\beta$ -CysFar.

(B) Confocal time-lapse images after microinjection of D-CysFar (left) and D-PalFar (right) in MDCK cells expressing Citrine-NRas.

(C) Ratiometric analysis of D-CysFar (left, n = 6) and D-PalFar accumulation at the Golgi (center, n = 6) with local Citrine-NRas used as a reference. Right: comparison of both.

(D) Microinjection of  $\beta$ -CysFar (left) and  $\beta$ -PalFar (right) in MDCK cells expressing Citrine-NRas.(E) Ratiometric analysis of  $\beta$ -CysFar (left, n = 4) and  $\beta$ -PalFar accumulation at the Golgi (center, n = 7) and comparison of both (right).All scale bars represent 10  $\mu$ m.

activity as described by previous biochemical assays. Scanning of multiple genomes with this consensus sequence revealed that the *Dictyostelium* genome contained only homologs of human

DHHCs 1–8, and while this organism has at least 11 Ras isoforms, none have a palmitoylatable cysteine. Therefore, if indeed Ras specific PAT activity exists, human HRas should not

become palmitoylated when expressed in *Dictyostelium discoideum*. Human HRas was however palmitoylated in *Dictyostelium* cells as indicated by its clear enrichment at the PM and certain internal membranes including endosomes (Figure 7E). The latter organelle that originates from the PM is abundantly present in *Dictyostelium* cells (Gerisch et al., 2004). The enrichment of HRas on the PM and endosomes was lost upon inhibiting palmitoylation with 2-bromopalmitate, similar to the effect on mammalian cells (Figure S3). FRAP kinetics showed that the relatively slow motility of HRas in *Dictyostelium* cells (Figure 7F) was consistent with that of palmitoylated HRas ( $t_{1/2} = 183.3 \pm 3.8$  s) as observed in mammalian cells (Figure 2E). These experiments show that no specific PAT activity exists for Ras and confirm the substrate tolerance of the palmitoylation machinery.

## DISCUSSION

In this study, we applied a chemical-biological approach to directly monitor dynamic palmitoylation in single cells. We uncovered the subcellular topography and the reaction dynamics of the core palmitoylation machinery in mammalian cells, thereby revealing a generic spatially organizing system that controls the subcellular localization of peripheral membrane proteins. Bulk palmitoylation occurs on the Golgi. This organelle provides directionality in the acylation cycle by allowing locally palmitoylated proteins to enter the secretory pathway from where they are targeted to the PM. Even these polylipidated proteins will eventually redistribute to all cellular membranes to reach equilibrium. This is countered by rapid and ubiquitous depalmitoylation that causes an increase in the effective diffusion of depalmitoylated proteins, and thereby mediates their continuous redirection to the Golgi from any given cellular membrane by local kinetic trapping. Remarkably, this de-/repalmitoylation machinery constitutes a spatially organizing system that does not require any form of direct ligand/receptor interaction in order to spatially segregate proteins. It dynamically maintains their spatial organization out of equilibrium by generating a directional flow from the Golgi to the PM. This counteracts the tendency of the system to increase its entropy by protein redistribution over all membranes. This directed transport acts like a conveyor belt along which palmitoylated peripheral membrane proteins are continuously enriched. The steady-state partitioning between Golgi and the PM with its interconnected endocytic compartment is dictated by the kinetics of palmitate turnover (Rocks et al., 2005) (Figures 5D, 3F, and 3G). Additional sorting signals or protein interactions could allow the palmitoylated proteins to access more specialized membrane subcompartments as for instance in neuronal cells (Huang and El-Husseini, 2005; Jura et al., 2006; Kang et al., 2008).

Numerous publications over the last few years have established the role of DHHC family proteins in protein palmitoylation in yeast and mammals. As anticipated for a typical enzyme, substrate specificity has been described for several of the DHHC proteins (Huang et al., 2009; Linder and Deschenes, 2007; Tsutsumi et al., 2008). These findings are mostly based on changes in the palmitoylation level of a putative substrate protein observed upon co-overexpression of DHHC proteins. Our study challenges the assumption that specific individual

PAT/substrate pairs are prerequisite in palmitate transfer. The experiments with D amino acids and nonnatural peptides clearly demonstrate that the sequence context flanking the target cysteine on the substrate does not contribute to substrate recognition. A recent study in yeast further supports the assumption of overlapping specificities (Hou et al., 2009). We thus propose that, in mammalian cells, any protein is qualified for palmitoylation that contains a surface-exposed and freely accessible cysteine that has transient access to Golgi membranes. This transient Golgi membrane proximity can be accomplished by nearby myristoyl or prenyl lipid anchors or nearby transmembrane domains, by binding to other proteins that permit transient Golgi accessibility or by an intrinsic weak membrane affinity.

No matter what type of substrate protein we tested—representatives of the three types of peripheral membrane proteins or, most importantly, probes with D amino acid configuration or nonnatural peptides—we always observed rapid palmitoylation only on the surface of the Golgi. This highly efficient core palmitoylation machinery rapidly processes any available target protein with very wide substrate tolerance. Palmitoylation activities on other subcellular sites such as the PM are feasible but would be relevant only for palmitoylatable proteins that do not have repeated access to the Golgi, like transmembrane proteins. Since our probes did not detect such activities, putative non-Golgi PATs must be far less efficient than the Golgi palmitoylation machinery or might involve additional specific offsite recognition that would prevent immediate turnover on the Golgi (discussed below). However, unlike in yeast, where PATs have been found on various different endomembrane systems (Hou et al., 2009; Ohno et al., 2006), all DHHC proteins in humans so far shown to be of enzymatic relevance localize at the Golgi (Fernández-Hernando et al., 2006; Huang et al., 2009; Ohno et al., 2006), with the exception of neuronal DHHC2 (Noritake et al., 2009).

Why are there 25 DHHC proteins in mammals? In our study we could rule out off-site recognition as an essential feature in the cellular palmitoylation reaction and, specifically, its involvement in the palmitoylation of Ras and of small palmitoylatable peptides. However, it might contribute to the efficiency of palmitoylation. There are no obvious motifs for such recognition on the DHHC proteins distal to their active site and/or the substrates distal to the target cysteine. Only three of the 25 DHHC family members contain protein interaction domains (SH3 on DHHC6 and ankyrin repeats on DHHC13 and 17), with DHHC5/8 and DHHC14 encoding potential PDZ binding motifs (type II and type I, respectively). Therefore, distal interaction would likely involve electrostatic or hydrophobic affinity but not structural recognition. Whether this is generally relevant or only applies to special cases such as the recently shown interaction between the yeast vacuole PAT Pfa3 and its substrate Vac8 (Hou et al., 2009; Nadolski and Linder, 2009) remains to be investigated. It is also noteworthy that at least some DHHC proteins might have biological functions independent of their PAT activity as has been shown recently for the yeast DHHC protein Swf1p in polarized secretion (Dighe and Kozminski, 2008).

Wide substrate tolerance is a known phenomenon in organic synthesis exploiting acylating and deacylating enzymes (Drauz and Waldmann, 2002). Therefore, a nonclassical enzymatic

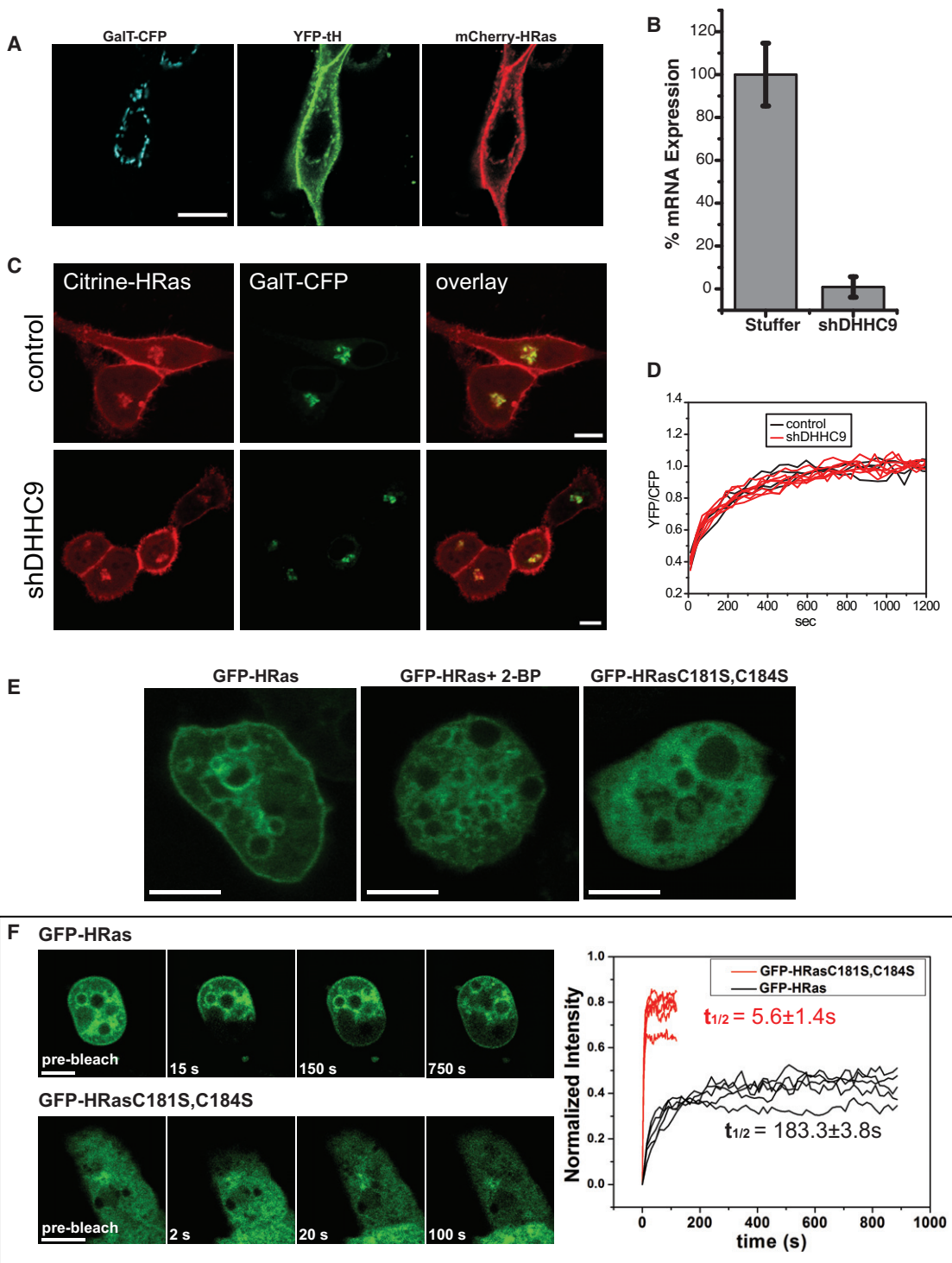


**Figure 7. HRas Does Not Require Distal Recognition or Specific PATs for Correct Localization**

(A) Comparison between the localization of full length HRas fused to mCherry and the C terminus of HRas fused to YFP. Equivalent distribution of the fragment versus full-length protein has a theoretical value of 1. Quantification of the experiment shows complete equivalence of both constructs ( $1.02 \pm 0.04$ ).

(B) Lentiviral shRNA-mediated downregulation of DHHC9 expressions in HeLa cells analyzed by quantitative RT-PCR with Actin B RNA used as reference. Error bars represent standard error of mean of percentages calculated from  $\Delta(\Delta Ct)$  values in three independent runs.

(C) Steady-state localization of HRas in DHHC9 knockdown and control HeLa cells.

(D) Fluorescence recovery after photobleaching of HRas at the Golgi in DHHC9 knockdown ( $n = 7$ ) and control ( $n = 4$ ) cells. The recovery of local fluorescence was ratiometrically quantified with GaIT-CFP used as a Golgi reference. Plateau values were normalized to one.

mechanism of palmitoylation is conceivable where DHHC proteins participate in a Golgi-based machinery that coordinates the accumulation, storage, relay and presentation of palmitoyl-CoA and accomplishes the bulk cellular palmitate transfer. DHHC proteins have been shown to be autoacylated (Lobo et al., 2002) and may establish a continuously preformed set of thioester-charged intermediates with high acylation potential. Once the acylated DHHC-protein encounters a substrate thiol, the thioesters are exchanged and the reaction would be driven by lateral diffusion and vesicular export of the product.

Do dynamic changes in palmitate turnover rates, as observed upon extracellular stimulation (El-Husseini et al., 2002; Kang et al., 2008), occur directly at the level of the PATs/thioesterase activity (Tsutsumi et al., 2008)? The fast kinetics and the lack of primary substrate specificity of the palmitoylation machinery as revealed in this study do not support this notion. However, regulation of palmitate turnover rates by extrinsic cues can very well arise indirectly from changes in the accessibility of thiol or thioester groups on the substrate protein, for example upon conformational changes of the substrate or upon masking or unmasking by other proteins. Likewise conceivable, stimulus-induced remodeling of the secretory pathway could alter the transport kinetics of palmitoylated proteins cycling between the Golgi and peripheral membranes. Such changes in substrate flow rates that will ultimately translate into altered apparent palmitate turnover rates might particularly be critical for palmitoylated proteins trafficking between Golgi outposts and dendritic spines in neuronal cells (Horton and Ehlers, 2003; Kang et al., 2008).

Our findings are relevant for drug discovery programs aimed at interference with aberrant signaling of palmitoylated proteins such as oncogenic Ras. Chemical compounds can now be identified that interfere with the palmitoylation machinery and thereby modulate oncogenic Ras signaling activity by affecting its spatial distribution (P.I.H.B. and H.W., unpublished data). Strategies to interfere with protein palmitoylation need to however consider the broad substrate tolerance in the palmitoylation reaction as delineated here.

## EXPERIMENTAL PROCEDURES

### Generation of Synthetic Lipopeptides

Lipopeptides synthesized on solid phase were purified, and their integrity was verified by liquid chromatography-mass spectrometry, MALDI-TOF, and proton nuclear magnetic resonance. Purification of relevant proteins and eGFP-Cys (eGFP with an additional C-terminal cysteine suitable for the MIC ligation), subsequent MIC coupling to the lipopeptides, and quality analysis by MALDI-TOF and SDS page was performed as described elsewhere (Bader et al., 2000) (for details, see the Extended Experimental Procedures). The NRas (1–181) protein was labeled prior to coupling with Cy3 monoreactive dye pack (Amersham Biosciences).

### Plasmid Constructs

Human HRas, NRas and mutants thereof, the MyrSer peptide, Fyn, GAP43, Galpha(1–10), RhoB, RRas, and TC10 were fused with fluorescent proteins

into mammalian expression vectors using conventional cloning techniques. Site-directed mutagenesis provided Cys to Ser mutant forms when necessary. For a detailed description of plasmid construction, see the Extended Experimental Procedures.

### Microscopy and Data Analysis

Confocal micrographs of various proteins and injected substrates were corrected for background, endomembrane cytosol volume filling factors, and segmented using masks for the relevant cellular compartments. Maximum intensities on these cellular compartments were normalized to one where appropriate and ratiometric traces were plotted against time where mentioned (for details, see the Extended Experimental Procedures).

### Cell Culture, Cell Transfection and 2-Bromopalmitate Treatment

MDCK cells were maintained in minimum essential medium supplemented with 10% fetal bovine serum (FBS), HeLa cells in Dulbecco's modified Eagle's medium (DMEM) with 10% FBS. Transient plasmid expression of MDCK cells was achieved by overnight transfection with Effectene (QIAGEN). HeLa cells were transfected with Fugene6 (Roche) for 6 hr and imaged 12 hr after transfection. For live cell microscopy, cells were cultured on 35 mm glass bottom dishes (MatTek, Ashland, MA). Transfected cells were serum starved for 5–6 hr in 1% FBS before all experiments and transferred to low-bicarbonate DMEM without phenol red supplemented with 25 mM HEPES (pH 7.4) for microscopy. 2-bromopalmitate (50 μM) was prediluted 1:100 before addition to the imaging medium.

## SUPPLEMENTAL INFORMATION

Supplemental Information includes Extended Experimental Procedures, seven figures, and three tables and can be found with this article online at doi: 10.1016/j.cell.2010.04.007.

## ACKNOWLEDGMENTS

O.R. received funding from the Human Frontier Science Program (LT Fellowship). We are thankful to C. Nowak and J. Luig for technical support, J. Lippincott-Schwartz, R. Tsien, M. Frame, and M. Torti for providing plasmids, and J. Moffat and Y. Fedyshyn for providing lentiviruses.

Received: September 18, 2009

Revised: January 8, 2010

Accepted: April 2, 2010

Published online: April 22, 2010

## REFERENCES

- Bader, B., Kuhn, K., Owen, D.J., Waldmann, H., Wittinghofer, A., and Kuhlmann, J. (2000). Bioorganic synthesis of lipid-modified proteins for the study of signal transduction. *Nature* 403, 223–226.
- Baker, T.L., Zheng, H., Walker, J., Collof, J.L., and Buss, J.E. (2003). Distinct rates of palmitate turnover on membrane-bound cellular and oncogenic H-ras. *J. Biol. Chem.* 278, 19292–19300.
- Bañó, M.C., Jackson, C.S., and Magee, A.I. (1998). Pseudo-enzymatic S-acylation of a myristoylated yes protein tyrosine kinase peptide in vitro may reflect non-enzymatic S-acylation in vivo. *Biochem. J.* 330, 723–731.
- Bijlmakers, M.J., and Marsh, M. (2003). The on-off story of protein palmitoylation. *Trends Cell Biol.* 13, 32–42.

(E) Representative images of *Dictyostelium* cells (1 of 20 each) expressing HRas and HRasC181S,C184S. HRas shows clear enrichment on the PM, which is lost upon treatment with 2-bromopalmitate.

(F) FRAP sequences of HRas and HRasC181S,C184S with representative examples (five each) in *Dictyostelium* cells showing the slower recovery of HRas, indicating its palmitoylated state.

Scale bars represent 5 μm. See also Figure S7.

- Bizzozero, O.A., Bixler, H.A., and Pastuszyn, A. (2001). Structural determinants influencing the reaction of cysteine-containing peptides with palmitoyl-coenzyme A and other thioesters. *Biochim. Biophys. Acta* 1545, 278–288.
- Charollais, J., and Van Der Goot, F.G. (2009). Palmitoylation of membrane proteins (Review). *Mol. Membr. Biol.* 26, 55–66.
- Choy, E., Chiu, V.K., Silletti, J., Feoktistov, M., Morimoto, T., Michaelson, D., Ivanov, I.E., and Philips, M.R. (1999). Endomembrane trafficking of ras: the CAAX motif targets proteins to the ER and Golgi. *Cell* 98, 69–80.
- Dighe, S.A., and Kozminski, K.G. (2008). Swf1p, a member of the DHHC-CRD family of palmitoyltransferases, regulates the actin cytoskeleton and polarized secretion independently of its DHHC motif. *Mol. Biol. Cell* 19, 4454–4468.
- Drauz, K., and Waldmann, H. (2002). Enzyme Catalysis in Organic Synthesis: A Comprehensive Handbook, Second Edition, Volume 2 (Weinheim, Germany: Wiley-VCH).
- El-Husseini, A.E., Craven, S.E., Chetkovich, D.M., Firestein, B.L., Schnell, E., Aoki, C., and Bredt, D.S. (2000). Dual palmitoylation of PSD-95 mediates its vesiculotubular sorting, postsynaptic targeting, and ion channel clustering. *J. Cell Biol.* 148, 159–172.
- El-Husseini, Ael-D., Schnell, E., Dakoji, S., Sweeney, N., Zhou, Q., Prange, O., Gauthier-Campbell, C., Aguilera-Moreno, A., Nicoll, R.A., and Bredt, D.S. (2002). Synaptic strength regulated by palmitate cycling on PSD-95. *Cell* 108, 849–863.
- Fernández-Hernando, C., Fukata, M., Bernatchez, P.N., Fukata, Y., Lin, M.I., Bredt, D.S., and Sessa, W.C. (2006). Identification of Golgi-localized acyl transferases that palmitoylate and regulate endothelial nitric oxide synthase. *J. Cell Biol.* 174, 369–377.
- Fishburn, C.S., Herzmark, P., Morales, J., and Bourne, H.R. (1999). Gbeta-gamma and palmitate target newly synthesized Galphaz to the plasma membrane. *J. Biol. Chem.* 274, 18793–18800.
- Fukata, M., Fukata, Y., Adesnik, H., Nicoll, R.A., and Bredt, D.S. (2004). Identification of PSD-95 palmitoylating enzymes. *Neuron* 44, 987–996.
- Gerisch, G., Benjak, A., Köhler, J., Weber, I., and Schneider, N. (2004). GFP-golvesin constructs to study Golgi tubulation and post-Golgi vesicle dynamics in phagocytosis. *Eur. J. Cell Biol.* 83, 297–303.
- Greaves, J., and Chamberlain, L.H. (2007). Palmitoylation-dependent protein sorting. *J. Cell Biol.* 176, 249–254.
- Greaves, J., Prescott, G.R., Fukata, Y., Fukata, M., Salaun, C., and Chamberlain, L.H. (2009). The hydrophobic cysteine-rich domain of SNAP25 couples with downstream residues to mediate membrane interactions and recognition by DHHC palmitoyl transferases. *Mol. Biol. Cell* 20, 1845–1854.
- Hirschberg, K., Miller, C.M., Ellenberg, J., Presley, J.F., Siggia, E.D., Phair, R.D., and Lippincott-Schwartz, J. (1998). Kinetic analysis of secretory protein traffic and characterization of golgi to plasma membrane transport intermediates in living cells. *J. Cell Biol.* 143, 1485–1503.
- Horton, A.C., and Ehlers, M.D. (2003). Dual modes of endoplasmic reticulum-to-Golgi transport in dendrites revealed by live-cell imaging. *J. Neurosci.* 23, 6188–6199.
- Hou, H., John Peter, A.T., Meiringer, C., Subramanian, K., and Ungeremann, C. (2009). Analysis of DHHC acyltransferases implies overlapping substrate specificity and a two-step reaction mechanism. *Traffic* 10, 1061–1073.
- Huang, K., and El-Husseini, A. (2005). Modulation of neuronal protein trafficking and function by palmitoylation. *Curr. Opin. Neurobiol.* 15, 527–535.
- Huang, K., Yanai, A., Kang, R., Arstikaitis, P., Singaraja, R.R., Metzler, M., Mullard, A., Haigh, B., Gauthier-Campbell, C., Gutekunst, C.A., et al. (2004). Huntingtin-interacting protein HIP14 is a palmitoyl transferase involved in palmitoylation and trafficking of multiple neuronal proteins. *Neuron* 44, 977–986.
- Huang, K., Sanders, S., Singaraja, R., Orban, P., Cijssouw, T., Arstikaitis, P., Yanai, A., Hayden, M.R., and El-Husseini, A. (2009). Neuronal palmitoyl acyl transferases exhibit distinct substrate specificity. *FASEB J.* 23, 2605–2615.
- Jura, N., Scotto-Lavino, E., Sobczyk, A., and Bar-Sagi, D. (2006). Differential modification of Ras proteins by ubiquitination. *Mol. Cell* 21, 679–687.
- Kang, R., Wan, J., Arstikaitis, P., Takahashi, H., Huang, K., Bailey, A.O., Thompson, J.X., Roth, A.F., Drisdale, R.C., Mastro, R., et al. (2008). Neural palmitoyl-proteomics reveals dynamic synaptic palmitoylation. *Nature* 456, 904–909.
- Kawase, K., Nakamura, T., Takaya, A., Aoki, K., Namikawa, K., Kiyama, H., Inagaki, S., Takemoto, H., Saltiel, A.R., and Matsuda, M. (2006). GTP hydrolysis by the Rho family GTPase TC10 promotes exocytic vesicle fusion. *Dev. Cell* 11, 411–421.
- Kuhn, K., Owen, D.J., Bader, B., Wittinghofer, A., Kuhlmann, J., and Waldmann, H. (2001). Synthesis of functional Ras lipoproteins and fluorescent derivatives. *J. Am. Chem. Soc.* 123, 1023–1035.
- Linder, M.E., and Deschenes, R.J. (2007). Palmitoylation: policing protein stability and traffic. *Nat. Rev. Mol. Cell Biol.* 8, 74–84.
- Lobo, S., Greentree, W.K., Linder, M.E., and Deschenes, R.J. (2002). Identification of a Ras palmitoyltransferase in *Saccharomyces cerevisiae*. *J. Biol. Chem.* 277, 41268–41273.
- Lu, J.Y., and Hofmann, S.L. (1995). Depalmitoylation of CAAX motif proteins. Protein structural determinants of palmitate turnover rate. *J. Biol. Chem.* 270, 7251–7256.
- Magee, A.I., Gutierrez, L., McKay, I.A., Marshall, C.J., and Hall, A. (1987). Dynamic fatty acylation of p21N-ras. *EMBO J.* 6, 3353–3357.
- Melkonian, K.A., Ostermeyer, A.G., Chen, J.Z., Roth, M.G., and Brown, D.A. (1999). Role of lipid modifications in targeting proteins to detergent-resistant membrane rafts. Many raft proteins are acylated, while few are prenylated. *J. Biol. Chem.* 274, 3910–3917.
- Mitchell, D.A., Vasudevan, A., Linder, M.E., and Deschenes, R.J. (2006). Protein palmitoylation by a family of DHHC protein S-acyltransferases. *J. Lipid Res.* 47, 1118–1127.
- Nadolski, M.J., and Linder, M.E. (2009). Molecular recognition of the palmitoylation substrate Vac8 by its palmitoyltransferase Pfa3. *J. Biol. Chem.* 284, 17720–17730.
- Navarro-Lérida, I., Alvarez-Barrientos, A., Gavilanes, F., and Rodriguez-Crespo, I. (2002). Distance-dependent cellular palmitoylation of de-novo-designed sequences and their translocation to plasma membrane subdomains. *J. Cell Sci.* 115, 3119–3130.
- Noritake, J., Fukata, Y., Iwanaga, T., Hosomi, N., Tsutsumi, R., Matsuda, N., Tani, H., Iwanari, H., Mochizuki, Y., Kodama, T., et al. (2009). Mobile DHHC palmitoylating enzyme mediates activity-sensitive synaptic targeting of PSD-95. *J. Cell Biol.* 186, 147–160.
- Ohno, Y., Kihara, A., Sano, T., and Igarashi, Y. (2006). Intracellular localization and tissue-specific distribution of human and yeast DHHC cysteine-rich domain-containing proteins. *Biochim. Biophys. Acta* 1761, 474–483.
- Paganini, S., Guidetti, G.F., Catricalà, S., Trionfini, P., Panelli, S., Balduini, C., and Torti, M. (2006). Identification and biochemical characterization of Rap2C, a new member of the Rap family of small GTP-binding proteins. *Biochimie* 88, 285–295.
- Pérez-Sala, D., Boya, P., Ramos, I., Herrera, M., and Stamatakis, K. (2009). The C-terminal sequence of RhoB directs protein degradation through an endo-lysosomal pathway. *PLoS ONE* 4, e8117.
- Quesnel, S., and Silvius, J.R. (1994). Cysteine-containing peptide sequences exhibit facile uncatalyzed transacylation and acyl-CoA-dependent acylation at the lipid bilayer interface. *Biochemistry* 33, 13340–13348.
- Rocks, O., Peyker, A., Kahms, M., Verveer, P.J., Koerner, C., Lumbierres, M., Kuhlmann, J., Waldmann, H., Wittinghofer, A., and Bastiaens, P.I. (2005). An acylation cycle regulates localization and activity of palmitoylated Ras isoforms. *Science* 307, 1746–1752.
- Rocks, O., Peyker, A., and Bastiaens, P.I. (2006). Spatio-temporal segregation of Ras signals: one ship, three anchors, many harbors. *Curr. Opin. Cell Biol.* 18, 351–357.
- Roth, A.F., Wan, J., Bailey, A.O., Sun, B., Kuchar, J.A., Green, W.N., Phinney, B.S., Yates, J.R., 3rd, and Davis, N.G. (2006). Global analysis of protein palmitoylation in yeast. *Cell* 125, 1003–1013.

- Sato, I., Obata, Y., Kasahara, K., Nakayama, Y., Fukumoto, Y., Yamasaki, T., Yokoyama, K.K., Saito, T., and Yamaguchi, N. (2009). Differential trafficking of Src, Lyn, Yes and Fyn is specified by the state of palmitoylation in the SH4 domain. *J. Cell Sci.* 122, 965–975.
- Seebach, D., Beck, A.K., and Bierbaum, D.J. (2004). The world of beta- and gamma-peptides comprised of homologated proteinogenic amino acids and other components. *Chem. Biodivers.* 1, 1111–1239.
- Shahinian, S., and Silvius, J.R. (1995). Doubly-lipid-modified protein sequence motifs exhibit long-lived anchorage to lipid bilayer membranes. *Biochemistry* 34, 3813–3822.
- Smotrys, J.E., and Linder, M.E. (2004). Palmitoylation of intracellular signaling proteins: regulation and function. *Annu. Rev. Biochem.* 73, 559–587.
- Smyth, P. (1997). Clustering sequences with hidden Markov models. *Adv. Neural Inf. Process. Syst.* 9, 648–654.
- Swarthout, J.T., Lobo, S., Farh, L., Croke, M.R., Greentree, W.K., Deschenes, R.J., and Linder, M.E. (2005). DHHC9 and GCP16 constitute a human protein fatty acyltransferase with specificity for H- and N-Ras. *J. Biol. Chem.* 280, 31141–31148.
- Takaya, A., Kamio, T., Masuda, M., Mochizuki, N., Sawa, H., Sato, M., Nagashima, K., Mizutani, A., Matsuno, A., Kiyokawa, E., and Matsuda, M. (2007). R-Ras regulates exocytosis by Rgl2/Rlf-mediated activation of RaIA on endosomes. *Mol. Biol. Cell* 18, 1850–1860.
- Tsutsumi, R., Fukata, Y., and Fukata, M. (2008). Discovery of protein-palmitoylating enzymes. *Pflugers Arch.* 456, 1199–1206.
- van't Hof, W., and Resh, M.D. (1997). Rapid plasma membrane anchoring of newly synthesized p59fyn: selective requirement for NH<sub>2</sub>-terminal myristylation and palmitoylation at cysteine-3. *J. Cell Biol.* 136, 1023–1035.
- Webb, Y., Hermida-Matsumoto, L., and Resh, M.D. (2000). Inhibition of protein palmitoylation, raft localization, and T cell signaling by 2-bromopalmitate and polyunsaturated fatty acids. *J. Biol. Chem.* 275, 261–270.
- Zeidman, R., Jackson, C.S., and Magee, A.I. (2009). Protein acyl thioesterases (Review). *Mol. Membr. Biol.* 26, 32–41.

#### Note Added in Proof

The data referred to throughout as “P.I.H.B. and H.W., unpublished data” are now in press: Dekker, F., Rocks, O., Vartak, N., Menninger S., Hedberg, C., Balaraman, R., Wetzel, S., Renner, S., Gerauer, M., and Schölermann, B. et al. (2010). Small molecule inhibition of APT1 affects Ras localization and signaling. *Nat. Chem. Biol.*, in press. Published online April 25, 2010. 10.1038/nchembio.362.

**EXTENDED EXPERIMENTAL PROCEDURES****Generation of Semi-synthetic Proteins (Related to Figures 2, 3, 4, 5, and 6 and Figures S1 S2, S3, S4, S5, and S6)****General Information**

Fmoc-4-hydrazinobenzoyl NovaGel resin with a loading of 0.56 mmol/g and 2-Chlorotriyl Novagel resin with a loading of 1.30 mmol/g were purchased from Novabiochem. HOBr anhydrous (N-hydroxybenzotriazole), HCTU (2-(6-chloro-1H-benzotriazole-1-yl)-1,1,3,3-tetramethylaminium hexafluorophosphate), HBTU (2-(1H-benzo-triazole-1-yl)-1,1,3,3,-tetramethylaminium hexafluorophosphate), DIPEA (N,N-diisopropyl-ethylamine), DMAP (4-dimethylamino-pyridine), DIC (N,N-diisopropyl-carbodiimid), IBCF (isobutyl-chloroformate), TEA (triethylamine), DMF (N,N-dimethylformamide) stored over molsieves, piperidine (redistilled), HATU (O-(7-azabenzotriazol-1-yl)-N,N,N',N'-tetramethyl-uronium hexafluorophosphate), 6-maleimidohexanoic acid (MIC), hexafluoroisopropanol (HFIP), triethylsilane (TES), trifluoroethanol (TFE),  $\alpha$ - and  $\beta$ -amino acids, allyl bromide, and myristoyl chloride were obtained from Sigma-Aldrich/Fluka.

**General Procedure for the Synthesis of Lipidated NRas Peptides (Related to Figure S1A)**

Commercially available Fmoc-4-hydrazinobenzoyl NovaGel resin was used for the solid-phase reactions. Anhydrous solvents were used for each reaction. The 50ml reactor flask had a frit at the bottom, a stopcock, which permitted rapid filtration and washing of the resin, and a side arm which allowed the supply of argon. The resin loading was determined by measuring the Fmoc groups. Cysteine building blocks, synthesized as described in the literature (Lumbierres et al., 2005), were coupled by using HBTU/HOBt/collidine (4:4:4) in CH<sub>2</sub>Cl<sub>2</sub>/DMF (1:1). All other amino acids were coupled by using HBTU/HOBt chemistry. Typically, the Fmoc-amino acid (AA) (4 eq) was treated for two minutes with HBTU (4 eq), HOBt (4 eq) in DMF, then DIPEA (8 equiv) was added and the solution was stirred for an additional two minutes. The solution was then added to the resin, which was subsequently agitated for 2-3h at room temperature. The completeness of the couplings reactions was monitored with the Bromophenolblue-Test. The Fmoc-group was removed by commercial available redistilled piperidine in anhydrous DMF (DMF:piperidine; 1:1) (3 times 5 min). Then the resin was washed five times with DMF, and the next coupling was carried out. After the incorporation of Fmoc-Cys(Pal)-OH, 2% DBU in DMF (2 times·60 s) was used for Fmoc deprotection and HATU in CH<sub>2</sub>Cl<sub>2</sub>/DMF (7:1) was used for the subsequent coupling of the amino acids, immediately after the washing steps. In the final step 6-maleimidohexanoic acid was coupled to the resin using HBTU/HOBt/DIPEA (4:4:8). After washing the resin 3 times with anhydrous CH<sub>2</sub>Cl<sub>2</sub>, the cleavage of the peptide was carried out with a cocktail of Cu(OAc)<sub>2</sub> (0.55 eq), pyridine (35 eq) and MeOH (215 eq) in anhydrous CH<sub>2</sub>Cl<sub>2</sub>. The mixture was agitated for 2.5h and the resin was washed 5 times with CH<sub>2</sub>Cl<sub>2</sub>. After washing the organic layer with water, the final peptides were obtained by preparative HPLC on an Agilent Series 1100/LC/MSD VL(ESI) and a VP 125/21 Nucleodur C4 Gravity column.

**General Procedure for the Synthesis of Lipidated G $\alpha$ i Peptides (Related to Figure S1B)**

A solution of FmocLys(NH<sub>2</sub>)OAll (1.4 mmol) and diisopropylethylamine (972  $\mu$ L, 5.6 mmol, 4 eq) in dry CH<sub>2</sub>Cl<sub>2</sub> (7 mL) was added to 2-chloro trityl resin (1.73 g, loading 1.3 mmol/g). The mixture was shaken for 16 hr. After filtration, the resin was washed with CH<sub>2</sub>Cl<sub>2</sub>/MeOH/DIPEA (17:2:1 v/v/v) for 30 min followed by 5 flow washes with dichloromethane, dimethylformamide, methanol and dichloromethane. The resin was dried at high vacuum over night and featured an amino acid loading of 0.41 g/mmol. The peptides were synthesized using standard solid phase peptide chemistry on a 0.1 mmol scale. Peptide couplings of amino acids and myristoylated Glycine were done with 4 eq. HCTU and 8 eq. DIPEA for 1 hr. The Fmoc deprotection was performed with 2% DBU and 2% piperidine in DMF, 3 times 10 min. The peptides were cleaved from the solid support with 5% TFA/ 2% TES in CH<sub>2</sub>Cl<sub>2</sub> for 1 hr. The crude product was coevaporated with toluene and without further purification submitted to coupling with 6-maleimidohexanoic acid (2 eq), using HATU (2 eq) and triethylamine (6 eq) for 16 hr in 5 ml DMF. After the evaporation of the solvent the crude product was dissolved in 50% TFA in CH<sub>2</sub>Cl<sub>2</sub> and stirred for 2 hr. After coevaporation with toluene the peptides were purified using an Agilent Series 1100/LC/MSD VL (ESI) and a VP 125/21 Nucleodur C4 Gravity column.

**General Procedure for the Synthesis of Lipidated Fyn Peptides (Related to Figure S1C)**

The peptides were synthesized using standard solid phase peptide chemistry on a Rink Amide MBHA resin on a 0.1 mmol scale. After an initial Fmoc deprotection 4 eq. Fmoc-Lys(Mtt)-OH were coupled with 4 eq. HCTU and 8 eq. DIPEA for 1 hr. Further peptide couplings of amino acids and myristoylated Glycine were done with 4 eq. HCTU and 8 eq. DIPEA for 1 hr. The Fmoc deprotection was performed with 2% DBU and 2% piperidine in DMF, 3 times 10 min. After assembly of the lipidated peptide on resin the Mmt protection group of lysine were deprotected with 65% DCM/ 20% hexafluoroisopropanol/ 10% trifluoroethanol/ 5% triethylsilane 3 hr. The deprotected side chain was directly coupled with 4 Equation 6-maleimidohexanoic acid, 4 eq. HCTU and 8 eq. DIPEA for 1 hr. The peptides were cleaved from the solid support with 95% TFA/ 2.5% TES/ 2.5% H<sub>2</sub>O for 3 hr. The crude product was coevaporated with toluene and were purified using an Agilent Series 1100/LC/MSD VL (ESI) and a VP 125/21 Nucleodur C4 Gravity column.

**Lipopeptide Coupling to NRas(1-181) and eGFP-Cys**

Purification of NRas (1-181) and other proteins and eGFP-Cys (eGFP with an additional C-terminal cysteine suitable for the MIC-ligation), subsequent coupling to the lipopeptides and quality analysis by MALDI-TOF and SDS page was performed as described elsewhere (Bader et al., 2000). The NRas (1-181) protein was labeled prior to coupling with Cy3 monoreactive dye pack (Amersham Biosciences). Briefly, 10 mg purified NRas were incubated with 2.5 times excess of Cy5 maleimide ester in 0.1 M NaCO<sub>3</sub>/NaHCO<sub>3</sub>, pH 9.3 for 1.5 hr on ice. After dialysis for 0.5 hr against 0.1 M NaCO<sub>3</sub>/NaHCO<sub>3</sub>, pH 9.3 another dialysis was performed over night against 20 mM Tris, 5 mM MgCl<sub>2</sub> pH 7.4.

**NMR, LC and ESI-MS Data of All Generated Peptides (Related to Tables S1, S2, and S3)**

The purity and integrity of the lipopeptides were analyzed and confirmed by LC/ESI-MS using a C4 column with a gradient from 20% - 100% in 15 min or by NMR.

**MALDI-TOF (Related to Tables S1 and S2)**

The ligated proteins were analyzed using MALDI-TOF. For the measurements the protein solutions were diluted with a sinapinic acid matrix (ACN saturated with sinapinic acid/ 0.3% TFA in H<sub>2</sub>O, 1:2).

**Plasmid Constructs**

mCitrine and mCFP fusions of HRas, NRas, HRasC181S and HRasC181S,C184S were described previously (Rocks et al., 2005). paGFP- and mCherry-fusions to HRas, NRas, HRasC181S and HRasC181S,C184S were obtained from mCFP fusions by replacing mCFP with Agel/BsrGI fragments of paGFP-C1 (gift from J. Lippincott-Schwartz) or mCherry-C1. Gαi1(1-10) fusions to paGFP, mCitrine and mCherry were generated by insertion of an EcoRI/Agel fragment encoding amino acids 1-10 of Gαi1 into paGFP-N1, mCitrine-N1 or mCherry-N1. mCherry-C1 and mCherry-N1 were generated by insertion of a Agel/BsrGI PCR fragment of mCherry cDNA (gift from R. Tsien) into pEGFP-C1 or pEGFP-N1. GalT, a Golgi marker, encodes a fragment of β-1,4-galactosyltransferase fused to mCFP. MyrCys-Citrine, MyrCys-paGFP, MyrSer-Citrine and MyrSer-paGFP were created by cloning of the linker fragment of Linker-GFP (Navarro-Lérida et al., 2002) into mCitrine-N1 and paGFP-N1. Fyn-GFP was a gift from M. Frame. Fyn-Citrine, was cloned using similar procedures as described above. Spel/BgIII fragments of human HRas wt and HRasC181S,C184S were cloned into the extra-chromosomal GFP expression vector pDM317 for expression in *Dictyostelium* under endogenous actin-15 promoter and an actin-8 terminator. Citrine-HRas179C,183C was obtained by site directed mutagenesis. mCitrine fusions of RhoB, RRas and TC10 were generated by insertion of respective full length cDNAs into mCitrine-C1. GFP-Rap2C was gift from M. Torti.

**Microscopy and Data Analysis (Related to Figures 1, 2, 3, 4, 5, and 6 and Figures S2, S3, S4, S5, and S6)**

Cells were maintained at 37°C if not stated otherwise. FRAP and microinjection experiments were performed on Leica TCS SP2 AOBS or Leica TCS SP5 microscopes, photoactivation experiments on an Olympus FV1000 microscope with a SIM scanner. FRAP experiments in DHHC9 knock down cells were performed on an Olympus FV1000 microscope at room temperature. The microscopes were equipped with a 63X/1.3 NA oil immersion lens and a temperature controlled chamber. CFP, paGFP and Citrine were excited by using the 457.9-nm, 488-nm and 514-nm Ar laser lines, respectively. mCherry and Cy3 were excited by using a 561-nm diode laser. Photoactivation of paGFP was achieved by using a 405-nm diode laser (Coherent).

Accumulation of microinjected lipoproteins at the Golgi or PM was quantified as the ratio of local Cy3 fluorescence (Cy3-labeled lipoprotein) to Citrine fluorescence (Citrine-NRas or Gα1(1-10)-Citrine). Masks of the Golgi and PM were generated from Citrine-NRas images. In order to correct for fluorescence contamination of the Golgi or the PM area, additional background masks were defined using regions right next to the Golgi or PM. The contamination arises from probe in the cytosol and on other colocalizing endomembranes (mainly endoplasmic reticulum), both occupying a substantial volume of the Golgi or PM areas. Average Cy3 and Citrine intensities in the Golgi, PM and background masks were measured and background was subtracted assuming an endomembrane-cytosol volume filling factor of 0.7. Ratios were then determined as:

$$(Cy3(\text{Golgi or PM}) - (\text{Cy3}(\text{background}) * 0.7)) / (\text{Citrine}(\text{Golgi or PM}) - (\text{Citrine}(\text{background}) * 0.7))$$

The maximum intensity of the Golgi curves was normalized to one, corresponding PM curves therefore reach lower plateau values. For quantitative assessment of the contrast of microinjected probe fluorescence at the Golgi over adjacent endomembranes/cytosol, the Cy3 intensity at the Golgi was divided by the Cy3 intensity in this adjacent region.

Fluorescence loss after photoactivation at the Golgi was quantified as the ratio of local paGFP to mCherry fluorescence. Golgi masks were obtained from images of the respective palmitoylatable construct fused to mCherry and background correction was performed like in the microinjection experiments. The initial peak intensities after photoconversion were normalized to one.

For ratiometric analysis of Golgi FRAP data from microinjection experiments, Citrine-NRas images were used to generate masks for the Golgi. GalT-CFP images acquired in parallel at every time-point were used to validate specific Golgi-localization of NRas. The masks were used to calculate the ratio of the sum of Cy3 intensity resulting from Cy3-labeled probes at the Golgi over the sum of Citrine-NRas intensity at each time point. Plateau values were normalized to one. Analysis of Golgi FRAP data of Citrine-HRas C181S,C184S was performed using Golgi masks derived from CFP-HRas images.

**Microinjection of Proteins**

Injection needles were prepared from borosilicate glass capillaries from Harvard Apparatus (Kent, UK), using a micropipette puller (Sutter Instruments P-97). Probes destined for microinjection were diluted in buffer (65 mM Tris, pH 7.5, 1 mM MgCl<sub>2</sub>) to a final concentration of 1-2 mg/ml. After centrifugation of fresh aliquots at 13000 g and 4°C for 15 min the supernatant was immediately used for injection. Microinjection was performed directly at the microscope using an automated micromanipulator (Eppendorf, Germany).

**RNAi and Quantitative RT-PCR (Related to Figures 7B–7D)**

Five different lentiviral shRNA targeting human DHHC9 (The RNAi Consortium, kind gift from J. Moffat) were screened for maximum downregulation in HeLa cells against control cells expressing empty pKLO.1 lentiviral expression plasmid ('stuffer', negative control). The following target sequence was used: GAGGAACTACCGCTACTTCTA.

HeLa cells were transfected with different lentiviral anti-DHHC9 shRNA expression, or stuffer sequences (negative control) were seeded in 35mm wells.  $1 \times 10^6$  cells were lysed and total RNA purified using the QIAGEN RNeasy Plus Mini Kit (Cat# 74106). During purification, the extracts were treated on column with QIAGEN RNase-free DNase (Cat# 79254). RNA concentrations were measured and purity verified spectrophotically by ensuring 260/280 ratios exceeded 1.96.

RT-qPCR was performed using the Quantitect SYBR Green RT-qPCR kit, using 250 ng total RNA from each cell line, and exon-overlapping primers for Actin B (reference) and DHHC9. Various primers were tested to ensure primer efficiencies were similar. RT-qPCR runs were performed twice for each sample, in triplicates per run.

ZDHHC9-For 5'-GGTCTCCGTGGTCAGGCCG-3'  
 ZDHHC9-Rev 5'-TGCCCTTTGCCGGCCATC-3'  
 ACTINB-For 5'-AAGATCAAGATCATTGCTCCTC-3'  
 ACTINB-Rev 5'-ATAAAAGCCATGCCAATCTC-3'

SYBR Green I fluorescence was quantified over 45 PCR cycles on Bio-rad iCycler thermocycler equipped with an iQ5 Optical Detection module. The fold-knockdown of DHHC9 mRNA as compared to cells transfected with Stuffer viruses was quantified using the modified delta(delta Ct) method.

#### Bioinformatics (Related to Figures 7E and 7F and Figure S7)

Full-length sequences of DHHC proteins derived from the UniProt database (2009) were used to generate a MUSCLE alignment (Edgar, 2004) and a Hidden Markov Model (HMM) (Smyth, 1997) was generated from this alignment (Figure S7A). The HMM was tested using the leave-one-out method to ensure lack of feature dependence on any one sequence, as well as statistically evaluated for scores on all DHHC proteins. The HMM-scores for the RasPATs were significantly higher than other DHHC proteins, and cladograms generated with the HMM alignment indicated that the putative RasPATs were more closely related to each other than to other DHHC proteins.

A PROSITE scan (de Castro et al., 2006) of all known genomes using the above mentioned consensus sequence derived from this HMM identified DHHC proteins 9, 14, 18, 17 in all available mammalian genomes (Figure S7B) and several other hits in organisms whose genomes are available but DHHC proteins have not yet been investigated. The *Dictyostelium discoideum* (Cellular Slime Mold) genome provided no hit for the putative RasPAT consensus sequence.

#### Dictyostelium Methods (Related to Figures 7E and 7F)

Wild-type *D.discoideum* strain Ax2 cells were grown axenically in HL5 medium at 22°C. Transformation of *D.discoideum* amoebae was accomplished by electroporation using supercoiled pDm317 plasmids. All transformants were maintained in G418 (20 µg/ml).

#### Sample Preparation

For vegetative *D.discoideum* cells, 50–200 µl of cell suspension from a confluent petridish was taken and added to 35mm MatTek dishes. Cells were allowed to attach for 15–20 min and washed twice with 17mM phosphate buffer (pH 6.5). Measurements were performed on cells incubated in buffer.

For FRAP experiments, amoeboid cells from a confluent dish were washed and redissolved in 4.8 ml phosphate buffer, plated on a 6 well non nutrient agar plate (800 µl/well), allowed to dry for 20 min and incubated for 6 hr at 22°C. For observation at higher magnification cells growing on top of non-nutritive agar were placed in a 35mm dish with cells facing down and imaged.

#### Fluorescence Recovery after Photobleaching (FRAP)

*D.discoideum* cells were prepared as described before and imaged on a Leica SP5 confocal microscope at room temperature. GFP was bleached at 488 nm, FRAP recovery image sequences were fitted to an exponential curve and fits were used for calculation of half-times of fluorescence recovery.

#### SUPPLEMENTAL REFERENCES

- Bader, B., Kuhn, K., Owen, D.J., Waldmann, H., Wittinghofer, A., and Kuhlmann, J. (2000). Bioorganic synthesis of lipid-modified proteins for the study of signal transduction. *Nature* 403, 223–226.
- de Castro, E., Sigrist, C.J., Gattiker, A., Bulliard, V., Langendijk-Genevaux, P.S., Gasteiger, E., Bairoch, A., and Hulo, N. (2006). ScanProsite: detection of PROSITE signature matches and ProRule-associated functional and structural residues in proteins. *Nucleic Acids Res.* 34 (Web Server issue), W362–W365.
- Edgar, R.C. (2004). MUSCLE: multiple sequence alignment with high accuracy and high throughput. *Nucleic Acids Res.* 32, 1792–1797.
- Lumbierres, M., Palomo, J.M., Kragol, G., Roehrs, S., Müller, O., and Waldmann, H. (2005). Solid-phase synthesis of lipidated peptides. *Chemistry (Easton)* 11, 7405–7415.
- Smyth, P. (1997). Clustering sequences with hidden Markov models. *Adv. Neural Inf. Process. Syst.* 9, 648–654.

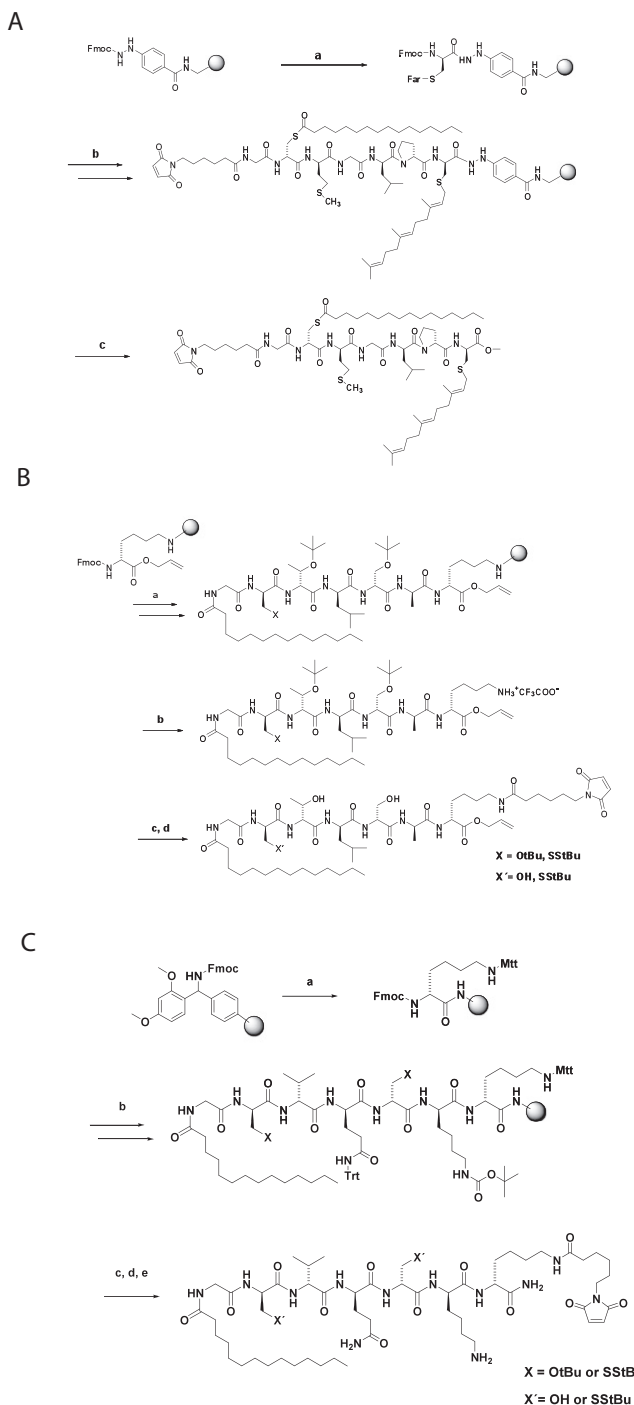


**Figure S1. General Synthesis Strategy for Lipidated Peptides, Related to Figures 2, 3, and 4**

(A) NRas peptides. a) DMF/piperidine (1:1), AA (4 eq), HOBr (4 eq), HBTU (4 eq), 2,4,6-collidine (4 eq) in DMF; b) SPPS: deprotection: DMF/piperidine (1:1) or DBU in DMF (2%), coupling: HBTU or HATU (4 eq), HOBr (4 eq), Fmoc-AA-OH (4 eq), DIPEA (8 eq) in DMF; c) Cu(OAc)<sub>2</sub>, (0.55 eq), pyridine (35 eq), MeOH (215 eq) in CH<sub>2</sub>Cl<sub>2</sub>.

(B) Gαi peptides. a) SPPS: deprotection: 2% DBU and 2% piperidine in DMF, coupling: HCTU (4 eq), Fmoc-AA-OH (4 eq), DIPEA (8 eq) in DMF; b) cleavage: 5% TFA / 2% TES in CH<sub>2</sub>Cl<sub>2</sub>; c) 6-maleimidohexanoic acid (2 eq), HATU (2 eq), triethylamine (6 eq) DMF; d) 50% TFA in CH<sub>2</sub>Cl<sub>2</sub>.

(C) Fyn peptides. a) Fmoc deprotection: 2% DBU/ 2% piperidine in DMF, coupling: Fmoc-Lys(Mtt)-OH(4 eq.), HCTU (4 eq), DIPEA (8 eq) in DMF; b) SPPS: deprotection: 2% DBU/ 2% piperidine in DMF, coupling: HCTU (4 eq), Fmoc-AA-OH (4 eq), DIPEA (8 eq) in DMF; c) 65% DCM/ 20% hexafluoroisopropanol/ 10% trifluoroethanol/ 5% triethylsilane d) 6-maleimidohexanoic acid (4 eq), HCTU (4 eq), DIPEA (8 eq) in DMF; e) 95% TFA/ 2.5% TES/ 2.5% H<sub>2</sub>O.

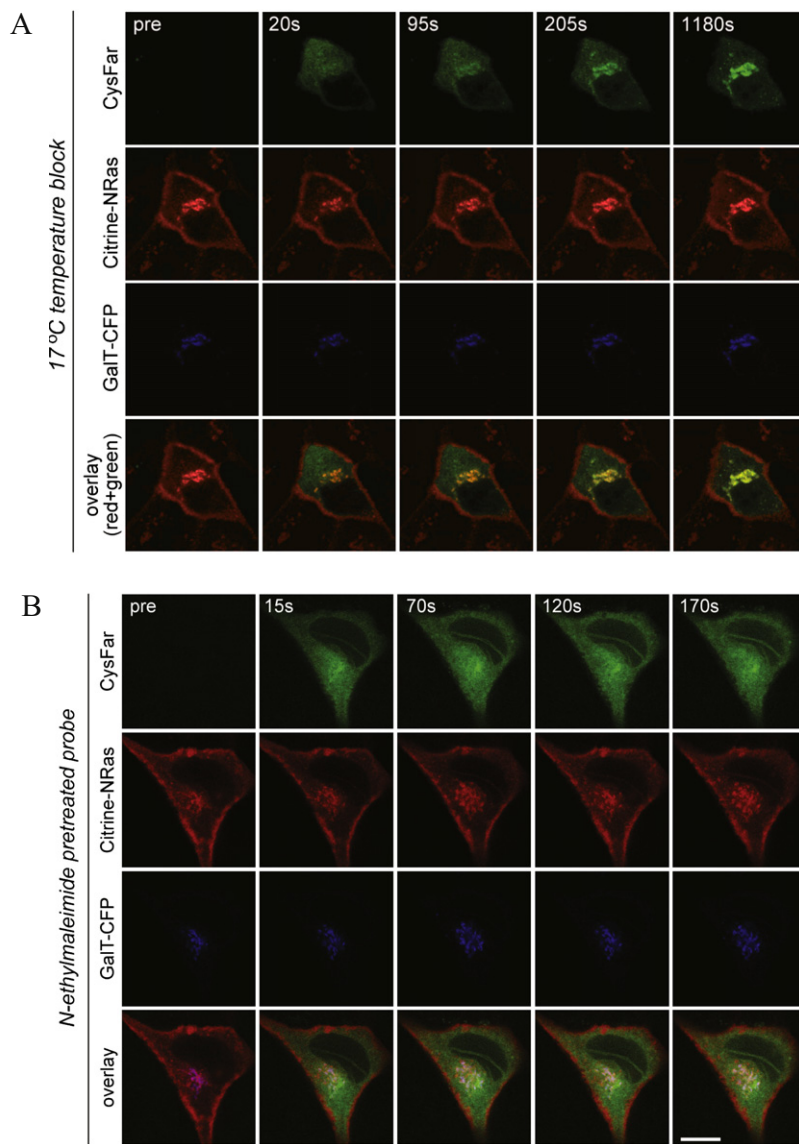


**Figure S2. CysFar Enrichment at the Golgi Occurs Due to Cysteine Palmitoylation with Subsequent Transport through the Secretory Pathway, Related to Figure 2**

(A) Temperature block of the exocytic pathway inhibits plasma membrane accumulation of semi-synthetic Ras probe CysFar: Time-lapse images of MDCK cells maintained at 17°C for 10 min prior and after microinjection of CysFar. This experiment shows that the secretory pathway re-directs palmitoylated Ras proteins to the plasma membrane.

(B) N-ethylmaleimide treatment of CysFar: Time-lapse images of MDCK cells coexpressing GalT-CFP and Citrine-NRas prior and after microinjection of CysFar incubated for 15 min before injection with 5 mM N-ethylmaleimide in order to covalently block potential free cysteine residues. This pre-treatment caused CysFar to randomly distribute over all membranes. Scale bars: 10 μM.

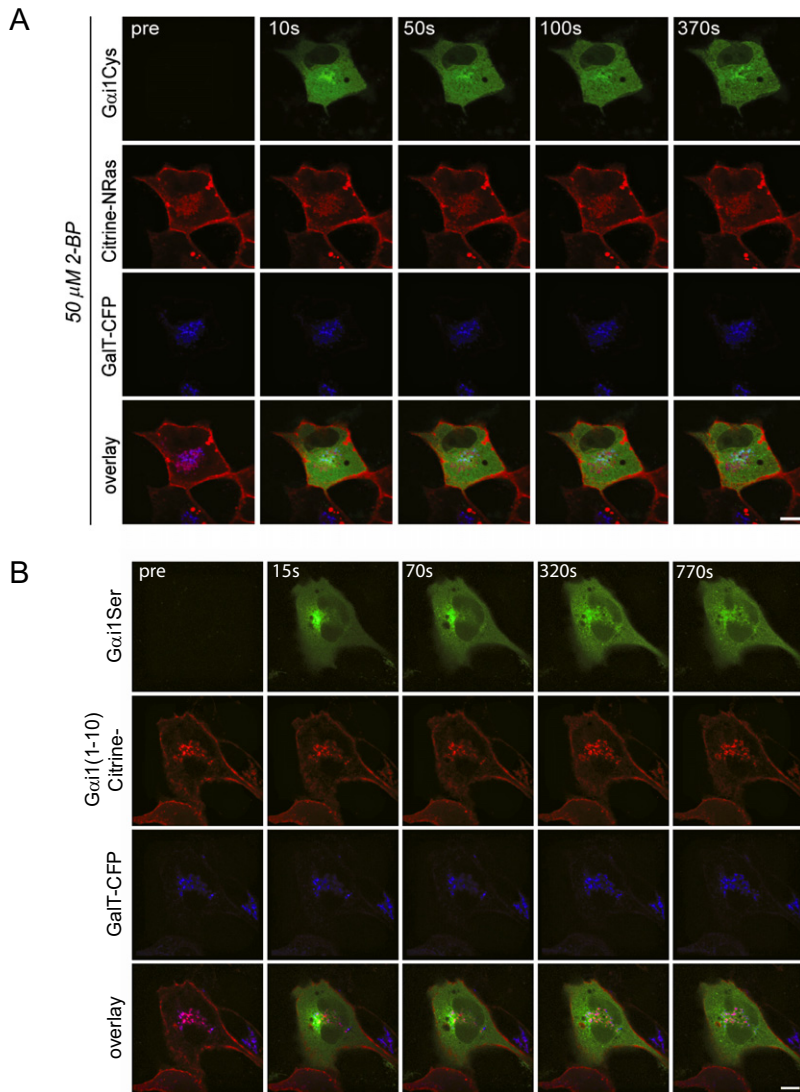


**Figure S3. 2-Bromopalmitate (2-BP) Inhibits Golgi Accumulation of G $\alpha$ i1Cys and Nonpalmitoylatable Serine Mutant of G $\alpha$ i1 Does Not Accumulate on the Golgi, Related to Figure 3**

(A) Time lapse images of MDCK cells incubated with 50 μM 2-BP for 40 min before and after microinjection with G $\alpha$ i1Cys. Note that 2-BP also causes redistribution of ectopically expressed Citrine-NRas. Inhibition of Ras palmitoylation is not instantaneous since 2-BP it is not a direct inhibitor of protein palmitoylation but acts upstream by interfering with lipid metabolism. Re-localization of palmitoylated Citrine-NRas to endomembranes can therefore be observed from 40 min onward after 2-bromopalmitate addition (see above). In the manuscript experiments are shown in the narrow time window where palmitoyl transfer activity is blocked but the PM/Golgi localization marker Citrine-NRas has not yet completely redistributed to endomembranes. Scale bars: 10 μM.

(B) Confocal time-lapse images of MDCK cells transiently expressing both the Golgi marker GaIT-CFP and Citrine fused to the first 10 amino acids of G $\alpha$ i1 before and after microinjection of G $\alpha$ i1Ser, showing that the lack of palmitoylation prevents Golgi enrichment of G $\alpha$ i1Ser.

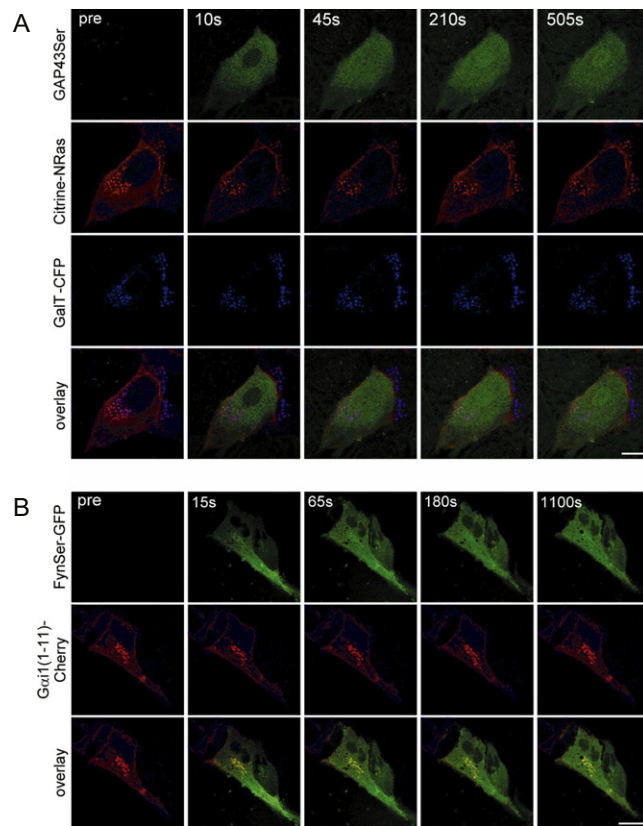


**Figure S4. Nonpalmitoylatable Serine Mutant Probes Do Not Accumulate on the Golgi, Related to Figure 3**

Confocal time-lapse images of MDCK cells transiently expressing both the Golgi marker GalT-CFP and Citrine-NRas before and after microinjection of GAP43Ser (A) or expressing G $\alpha$ i1(1-11)-Cherry after microinjection with FynSer-GFP (B). Scale bars: 10  $\mu$ M.

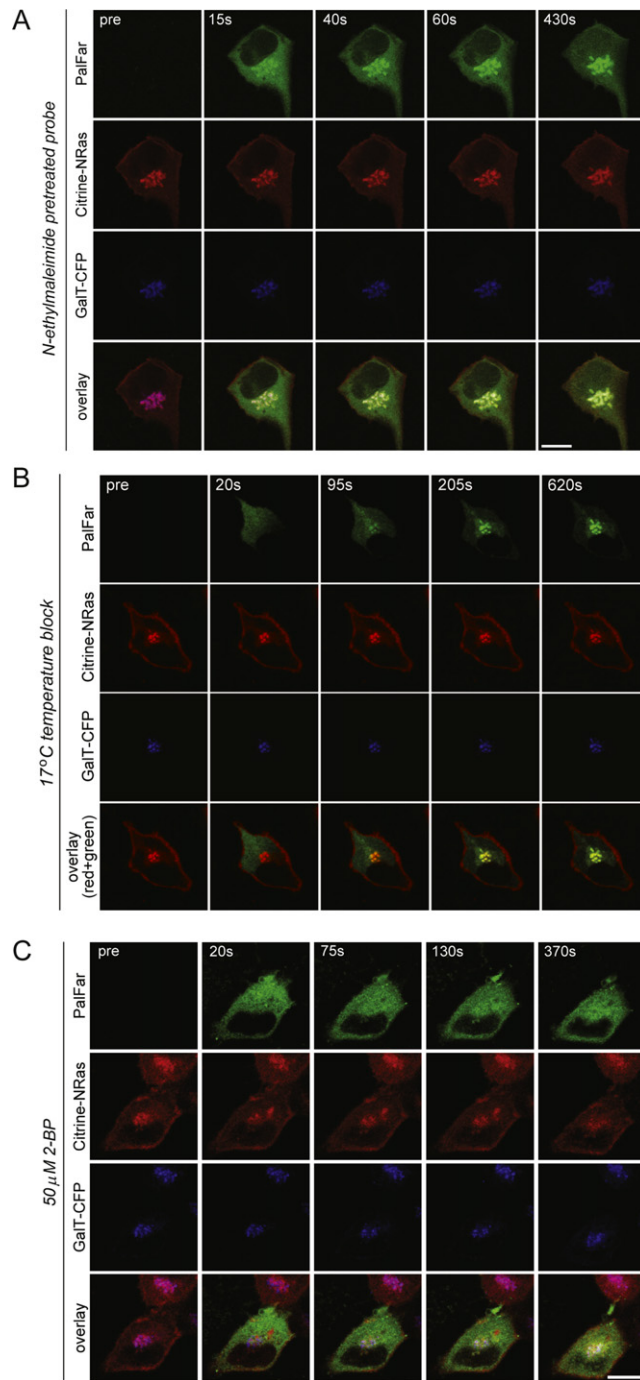


**Figure S5. Ubiquitous Depalmitoylation Precedes Repalmitoylation of PalFar at the Golgi, Related to Figure 4**

(A) Time-lapse images of MDCK cells coexpressing Galt-CFP and Citrine-NRAs prior to and after microinjection of semi-synthetic PalFar, incubated for 15 min before injection with 5 mM N-ethylmaleimide in order to covalently block potential free cysteine residues. This pre-treatment caused CysFar (see Figure S2B) to randomly distribute over all membranes while specific membrane trapping of PalFar still occurred. This demonstrates that rapid Golgi accumulation of PalFar is not due to contamination with unpalmitoylated probe. Scale bars: 10  $\mu$ M.

(B) Temperature block of the exocytic pathway inhibits accumulation of Ras probe PalFar: Time-lapse images of MDCK cells maintained at 17°C for 10 min prior and after microinjection of PalFar.

(C) Time lapse images of MDCK cells incubated with 50  $\mu$ M 2-BP for 40 min before and after microinjection with PalFar. Note that 2-BP also causes redistribution of ectopically expressed Citrine-NRAs. This experiments shows that PalFar must be depalmitoylated and then repalmitoylated for enrichment on the Golgi.

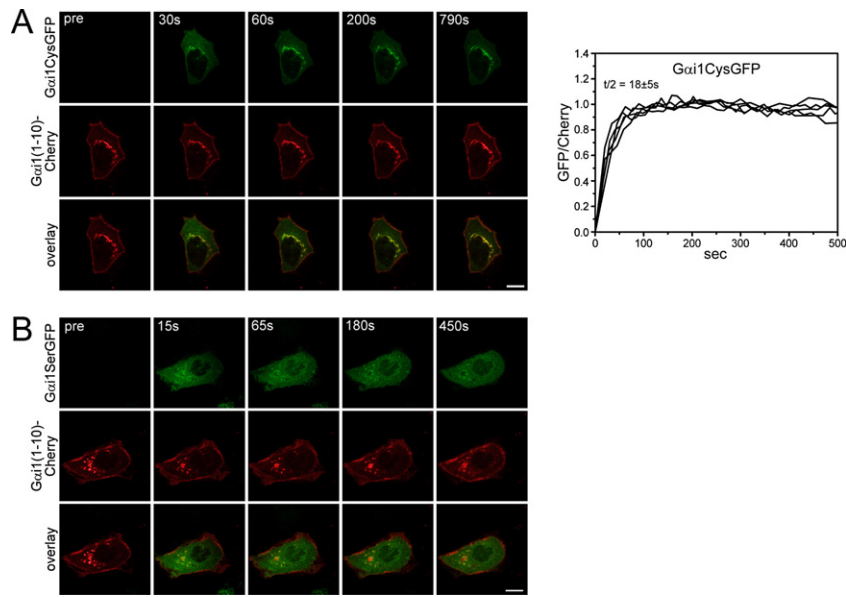


**Figure S6. Rapid Palmitoylation of G $\alpha$ i1-GFP on the Golgi, Related to Figures 3 and 5**

Time-lapse images of MDCK cells expressing G $\alpha$ i1(1-10) prior and after microinjection of G $\alpha$ i1Cys-GFP (A, left panel) or G $\alpha$ i1Ser-GFP (B). Scale bars: 10  $\mu$ M. Right panel: quantitative ratiometric analysis of G $\alpha$ i1Cys-GFP accumulation at the Golgi ( $n = 5$ ).

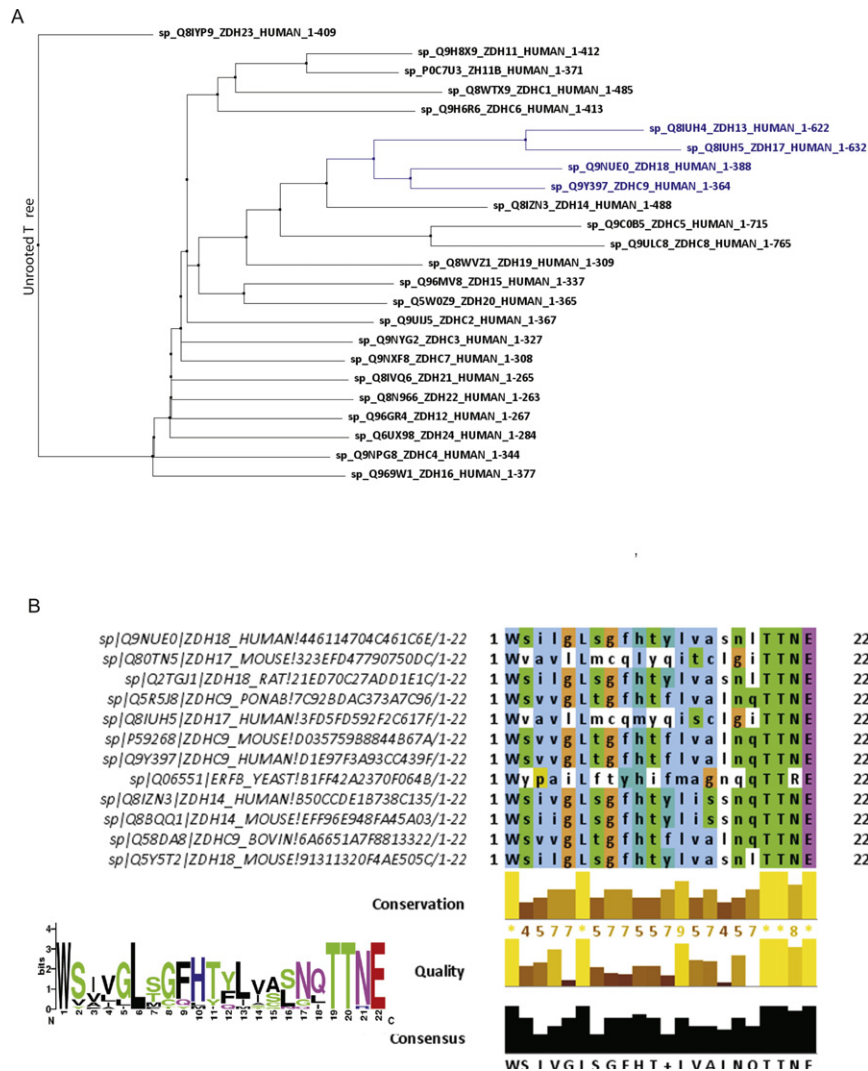


**Figure S7. Bioinformatics Analysis of DHHC Proteins, Related to Figures 7E and 7F**

(A) Phylogenetic tree showing human DHHC proteins as classified by the HMM. The tree is unrooted since no assumptions of an ancestral DHHC sequence have been made. The clade containing biochemically ascribed RasPATSs is indicated in blue.

(B) Alignment in the region of the consensus sequence of mammalian and yeast genome hits identified by the PROSITE scan of 'W-X4-L-X12-TTNE', showing high degree of conservation and fidelity.